Journal of Medicinal Chemistry

Article

Identification of non-competitive inhibitors of cytosolic 5'-nucleotidase II using a fragment-based approach

Zsuzsanna Marton, Rémi Guillon, Isabelle Krimm, Preeti Preeti, Rahila Rahimova, David Egron, Lars Petter Jordheim, Nushin Aghajari, Charles Dumontet, Christian Périgaud, Corinne Lionne, Suzanne Peyrottes, and Laurent Chaloin

J. Med. Chem., **Just Accepted Manuscript** • DOI: 10.1021/acs.jmedchem.5b01616 • Publication Date (Web): 24 Nov 2015

ACS Publications

Journal of Medicinal Chemistry is published by the American Chemical Society.
1155 Sixteenth Street N.W., Washington, DC 20036

Identification of non-competitive inhibitors of cytosolic 5'-nucleotidase II using a fragment-based approach

Zsuzsanna Marton[†,¶], Rémi Guillon[‡,¶], Isabelle Krimm[§], Preeti[‖], Rahila Rahimova[†], David Egron[‡], Lars P. Jordheim[⊥], Nushin Aghajari[‖], Charles Dumontet[⊥], Christian Périgaud[‡], Corinne Lionne[†], Suzanne Peyrottes[‡] and Laurent Chaloin[†,*]

[†] Centre d'études d'agents Pathogènes et Biotechnologies pour la Santé (CPBS), FRE 3689 CNRS - Université Montpellier, 1919 route de Mende, 34293 Montpellier cedex 5, France.

[‡] Institut des Biomolécules Max Mousseron (IBMM), UMR 5247 CNRS – Université Montpellier - ENSCM, Campus Triolet, cc1705, Place Eugène Bataillon, 34095 Montpellier cedex 5, France.

[§] Institut des Sciences Analytiques, UMR 5280 CNRS, Université Lyon 1, ENS de Lyon, 5 rue de la Doua, 69100 Villeurbanne, France.

[‖] Institut de Biologie et Chimie des Protéines FR3302, Molecular and Structural Bases of Infectious Diseases UMR 5086 CNRS – Université Lyon 1, 7 Passage du Vercors, 69367 Lyon, France.

[⊥] Université Lyon 1, Centre de Recherche en Cancérologie de Lyon, INSERM U1052, CNRS UMR 5286, Centre Léon Bérard, 69008 Lyon, France.

ABSTRACT

We used a combined approach based on Fragment-Based Drug Design (FBDD) and *in silico* methods to design potential inhibitors of the cytosolic 5'-nucleotidase II (cN-II), which has been recognized as an important therapeutic target in hematological cancers. Two sub-groups of small compounds (including adenine and bi-aryl moieties) were identified as cN-II binders and a fragment growing strategy guided by molecular docking was considered. Five compounds induced a strong inhibition of the 5'-nucleotidase activity *in vitro*, and the most potent ones were characterized as non-competitive inhibitors. Biological evaluation in cancer cell lines showed synergic effect with selected anticancer drugs. Structural studies using X-ray crystallography lead to the identification of new binding sites for two derivatives and of a new crystal form showing important domain swapping. Altogether, the strategy developed herein allowed identifying new original non-competitive inhibitors against cN-II that act in a synergistic manner with well-known antitumoral agents.

INTRODUCTION

To efficiently block an enzymatic function, one approach consists in the development of structure-guided inhibitors that will fit in the active binding site or known regulatory sites. Taking into account that substrate binding sites of enzymes exhibit quite complex shapes, Fragment-Based Drug Design (FBDD) represents a powerful strategy for the identification of such compounds[1-5] (for a detailed overview, see the recent review by Chen et al.).[6] Thus, fragment screening has been increasingly used for generating novel starting-points in drug

discovery programs. The use of small chemical entities (molecular weights beneath 300 Da), called fragments, facilitates the discovery of drug candidates by taking the advantage of the high quality interactions of the fragments within binding pockets of a protein, leading to high ligand efficiencies. In this respect, NMR and X-ray crystallography are the most frequently used screening tools,[7] even though surface plasmon resonance (SPR) and isothermal titration calorimetry (ITC) are also employed.[8] Initially applied to target soluble proteins, the FBBD approach has now been successfully extended to membrane proteins,[9,10] and nucleic acids.[11]

Here, we applied the FBDD approach to the design of inhibitors against the 5'-cytosolic nucleotidase II (cN-II). This protein catalyzes the hydrolysis of purine nucleoside 5'-monophosphates (NMP) into nucleosides and inorganic phosphate in order to regulate intracellular nucleotide pools. cN-II belongs to the large halo-acid deshydrogenase (HAD) family including eight 5’-nucleotidases with various cellular localization and substrate specificity. 5’-nucleotidases are also present in bacteria making them attractive targets for drug design as previously described using a similar approach.[12,13] The human cN-II is also involved in the resistance mechanism of some anti-cancer treatments based on cytotoxic nucleoside analogs.[14] Indeed, a high level of cN-II expression in blasts was found to be predictive of a worse patient outcome after cytarabine-based treatment of acute myeloid leukemia (AML).[15,16] Recently, mutants of cN-II, with hyperactive enzymatic activity, have been shown to be associated with resistance to chemotherapy in relapsed patients with acute lymphoblastic leukemia (ALL).[17,18] cN-II is also known as high-K_M nucleotidase II and therefore the inhibitors derived by analogy to the substrate exhibited elevated inhibition constants (millimolar range).[19-21] This enzyme represents a difficult target for classical approaches of drug design due to both a low affinity for

its substrate and a complex allosteric regulation. At least, two effector sites were identified by kinetics and crystallography,[22,23] showing that cN-II can be regulated through the binding of small regulators such as ATP, BPG or Ap_4A. In this respect, FBDD approach was applied to cN-II using the NMR screening of a chemical library of fragments, the building of their assemblies using molecular modeling, followed by synthesis, *in vitro* inhibition, biological assays in cancer cell models and structural studies.

RESULTS

NMR screening of the fragment library

A chemical library composed of 300 fragments was screened by NMR using recombinant purified human cN-II. Two NMR experiments were performed (STD and Waterlogsy) with mixtures of five fragments. From the positive pools, the fragment hits were then tested alone and only those showing binding signals in both experiments were confirmed as hits (Figure S1, Supporting information). A relatively high hit rate (10%) was obtained with this ligand-observed NMR screening approach, which is known to identify very weak binders. The fragment hits could be divided into two groups and representative structures are shown in Table 1. The first group contains aromatic and nitrogen-containing heterocylces, while the second one contains scaffolds reported in the literature as frequent-hitter privileged binding motives, such as the bi-phenyl motif.

Table 1: Representative fragments from the two groups identified as cN-II binders by NMR screening. F_{STD} indicates the amplification factor measured by STD and fragment **F4** is shown as a negative control.

Fragment #	Structure	F_{STD}	Inhibition at 1 mM (%)	Fragment #	Structure	F_{STD}	Inhibition at 1 mM (%)
Group n°1				*Group n°2*			
F1		0.5	23 ± 5	**F8**	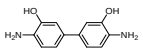	<0.5	23 ± 4
F2		3	30 ± 17	**F9**	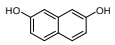	6.6	40 ± 6
F3	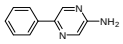	6	35 ± 3	**F10**	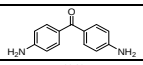	2.7	19 ± 3
F4		0	0.5 ± 1	**F11**		4.2	36 ± 5
F5		5.5	11 ± 9	**F12**	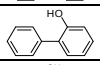	6.4	19 ± 1
F6		4.3	36 ± 5	**F13**		3.1	2 ± 1
F7		<0.5	19 ± 1	**F14**	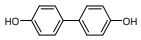	7.2	8 ± 2

The latter are highly hydrophobic and no consensus was observed for the chemical functions attached to the aromatic rings. The first group contained purine-based fragments with low STD factors (derived from **F1** or **F7**) and a wide range of nitrogen-based heterocycles, such as quinoline (**F2**), "phenyl-pyrazinyl" (**F3**) and "phenyl-imidazole" (**F6**) scaffolds with F_{STD} values ranging from 3 to 6 (Table 1). Furthermore, the heterocyclic ring was preferentially aromatic, as fragment **F4** was not detected as a ligand in contrast to **F3** (therefore, **F4** was not selected for the next steps). Interestingly, 1-H-benzimidazol-2-yl-methanol (**F5**), structurally closed to a purine scaffold, was also found to bind cN-II. The second group is composed of hydrophobic derivatives, mainly containing bi-aryl (for instance, **F10**, **F12** and **F14**) and naphthalene (**F9**) scaffolds with F_{STD} values between 2.7 and 7.2. This suggests the presence of a hydrophobic pocket where they may bind. In addition, we noticed that the presence of a polar group as substituent drastically changes the STD signal and therefore, the binding strength for these bi-

aryl fragments. Indeed, hydroxyl groups were more favored (**F12** or **F14**) than amino groups (**F10** or **F11**) and even more preferable than the combination of these (**F8**). Competition experiments with fragments could not be performed due to the lack of an identified competitor, as even IMP and inosine appear as very weak ligands (IMP is rapidly hydrolyzed into inosine, which is known to have a very weak affinity of 3-4 mM). Nevertheless, INPHARMA experiments were performed to assess whether the fragments share the same binding site as AdiS, an anthraquinone-like cN-II inhibitor previously identified by virtual screening.[24] Its affinity for cN-II was determined by kinetics by means of its K_i value of 2 ± 0.2 mM. As illustrated in Figure S2 (Supporting information), interligand NOEs were observed between fragments and AdiS. This result constitutes an experimental evidence that these two fragments (**F3** and **F10**) are able to bind into the IMP binding site of the enzyme since the AdiS inhibitor was previously characterized as a competitive inhibitor.

cN-II inhibition by hit fragments

Fragments identified by ligand-observed NMR experiments were further evaluated by enzymatic inhibition assays using the purified recombinant enzyme in order to validate the most interesting fragments. Most of them were able to inhibit hydrolysis of IMP when used at high concentrations. However, due to solubility issues for concentrations higher than 2 mM, the IC_{50} could not be determined and a comparison of their effect at 1 mM was used as indicator of inhibitory activity (Table 1). The most efficient fragment (40 ± 6% of inhibition) was 2,7-dihydroxynaphthalen (**F9**), followed by bi-aryl-related compounds harboring two six-membered aromatic rings (≥ 35% of inhibition) such as 5-phenyl-2-pyrazinylamine (**F3**) and 2-biphenyl-

amine (**F11)**. This result was confirmed by the moderate effect (~20% of inhibition) observed with structurally related fragments including a biphenyl or a benzophenone motif (**F8**, **F12**, **F14** and **F10**, respectively). Amongst the first group, several fragments were able to significantly inhibit cN-II such as adenine (**F7**) and 2-amino-6-chloropurine (**F1**). Similarly, inhibition was observed for the other nitrogen-containing aromatic rings (**F2**) and with a weaker effect for **F5**. Another interesting substructure in this group was also detected as a cN-II inhibitor, and corresponds to the association of a phenyl group and an imidazole moiety (**F6**), thus displaying a common chemical feature with the bi-aryl subgroup. Interestingly, when the two phenyl groups were separated by freely rotatable bonds such as for compound **F13**, it was completely inactive. This suggests that the flexibility and/or the distance between the two rings may be important. Finally, the most promising fragment in this group was the biphenyl amine (**F11**) with a single bond between both aromatic rings. In agreement with its low F_{STD} value, the fragment **F4** was found to be totally inactive, whereas fragment **F8** was partially able to inhibit cN-II despite its low F_{STD} value.

In silico binding prediction of the hit fragments

Based on the results of NMR experiments and of the *in vitro* inhibition assays, the most promising fragments were composed of the following scaffolds: “C-6-substituted purine”, “naphtalene”, “bi-aryl”, “phenyl-imidazole” and “quinoline”. In order to guide the assembly, merging or growing process, a molecular docking study (Figure 1) was performed in the enzyme active site (as INPHARMA experiments indicated that the fragments bind to the IMP site).

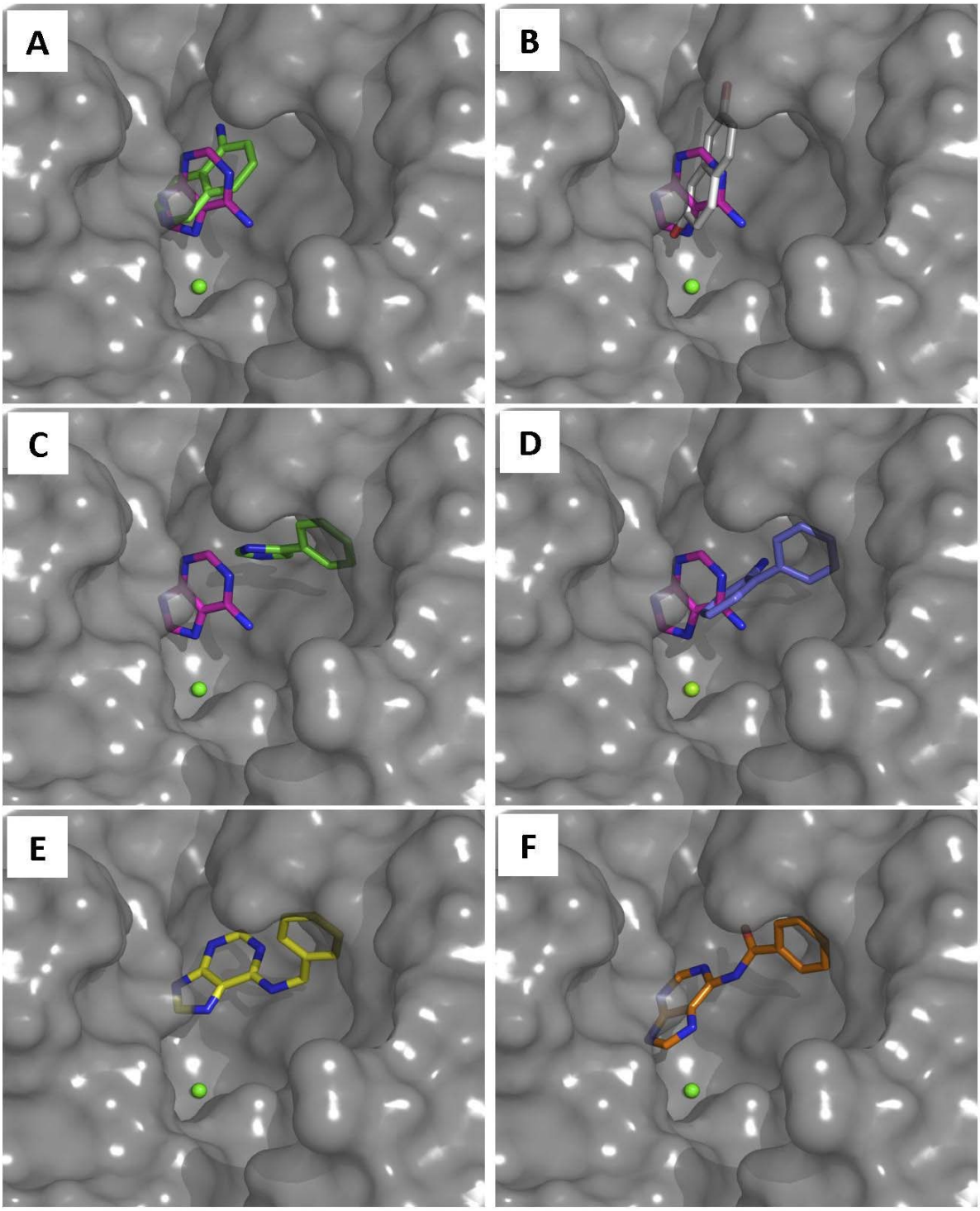

Figure 1: Molecular docking of the most representative hit fragments on the cN-II crystal structure (2XCW, shown as solvent accessible surface with the magnesium ion depicted as a green sphere). Superimposition of docking poses obtained with **adenine** (or **F7** in stick

representation and carbon atoms in magenta) and (A) **F2** (quinoline, green) or (B) **F9** (naphthalene, light grey) showing overlapping areas. Overlay of the binding poses obtained with **adenine** (magenta) and (C) **F6** (light green) or (D) **F11** (dark blue) fragments showing two distinct binding areas. (E) *N*-6-benzyl-adenine (**F15**, yellow) and (F) *N*-6-benzoyl-adenine (**F16**, orange) binding poses.

Steric hindrance was predicted between adenine (**F7**) and quinoline (**F2**) or naphthalene (**F9**) fragments (Figure 1A and B). A partial overlap was also observed with the 4,4'-diamino-benzophenone (**F10**, data not shown). In contrast, phenyl-imidazole (**F6**) or bi-aryl (**F11**) compounds (Figure 1C and D) were predicted to bind to a different cavity near the adenine site. The purine fragment was repeatedly found to be deeply inserted near the magnesium ion in contrast to phenyl or bi-aryl containing fragments which appeared to bind to a more exposed area (usually occupied by inosine). From the docking results, two sub-pockets were identified in which adenine and phenyl groups can be accommodated. Therefore, we searched for commercially available and structurally related compounds that combine these two scaffolds and evaluated their binding mode. As shown in Figure 1E and F, the binding mode for *N*-6-benzyl-adenine (**F15**) and *N*-6-benzoyl-adenine (**F16**) was found to be compatible with the ones of adenine and phenyl moieties (see structure of **F15**-**F16** in Figure 2). Moreover, the nature of the linker between these two scaffolds seems to have a direct effect on the adenine location (more buried in the case of *N*-6-benzoyl-adenine). Thus, the most interesting association appeared to be *N*-6-benzoyl-adenine (**F16**). These two compounds were assayed by NMR and both were detected as cN-II ligands using STD and Waterlogsy experiments as illustrated in

Figure 2. The F_{STD} values for the protons are related to their solvent accessibility: the lower the F_{STD} value, the higher the solvent accessibility of the proton upon binding to the protein target.

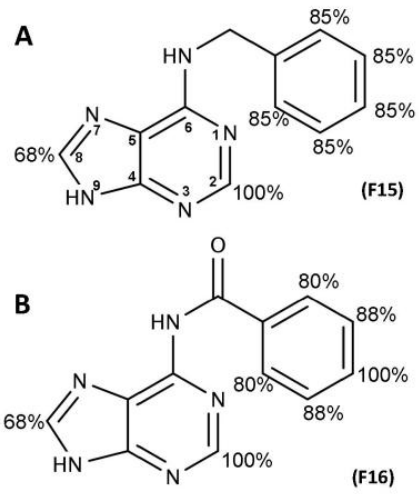

Figure 2: Per-proton F_{STD} percentages for the two larger fragments, *N*-6-benzyl-adenine or **F15** (A) and *N*-6-benzoyl-adenine or **F16** (B) showing the different solvent accessibility of the protons (highest STD percentages indicate protons deeply buried in the protein binding site).

If we analyze the docking pose of **F16** (Figure 1F), and compare with F_{STD} values, the proton in position C8 (68%) of the adenine moiety is solvent exposed as compared to the proton in position C2 (100%). Regarding the phenyl ring, the proton in *para* position (100%) is more buried than the other ones (80 or 88%). These comparisons between docking and STD data are in perfect agreement. For compound **F15**, due to spectral overlap, the difference of accessibility of the various phenyl protons could not be measured accurately but the proton in position C8 (68%) of the adenine moiety is observed as solvent exposed while the proton in position C2 (100%) is buried (Figure 2). Thus, *N*-6-benzyl-adenine (**F15**) and *N*-6-benzoyl-adenine (**F16**) were

further evaluated for their cN-II inhibition capacity. Both compounds exhibited a moderated inhibition of cN-II activity (20 ± 6 and 28 ± 2% of inhibition at 1 mM for **F15** and **F16**, respectively), confirming our docking-guided hypothesis.

Synthesis of the targeted compounds

According to all data obtained from NMR binding, *in vitro* activity, molecular docking and group epitope mapping, a generic chemical structure was proposed based on the most interesting fragments (Figure 3). We explore the chemical diversity through the relative position of the two phenyl groups (*ortho*, *meta* and *para* or fused), as well as the position and the nature of the five-membered nitrogen-containing heterocycle.

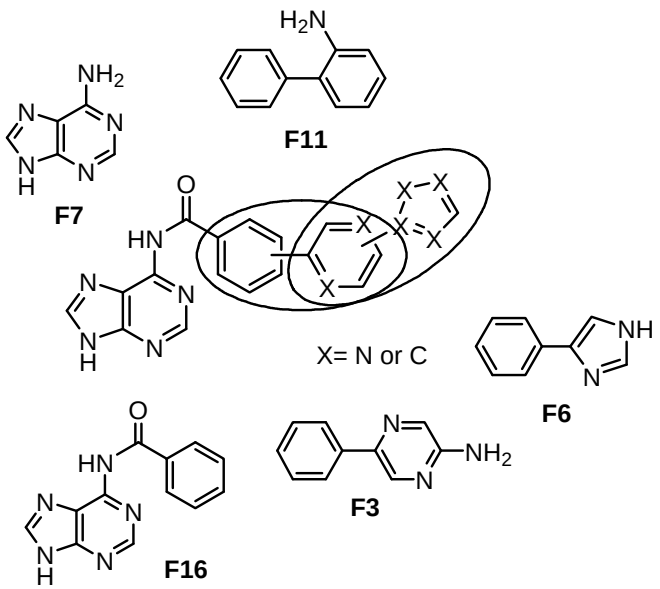

Figure 3: Retained strategy for fragment growing starting from adenine and linking with two merged structural scaffolds (bi-aryl and phenyl-imidazole) as shown by the three circles.

This strategy for chemical synthesis allowed both to focus on the major sub-groups previously identified and to include diversity in the merging process. In this respect, final compounds may incorporate *N*- or *C*-branched imidazole as well as pyrrole moieties (Table 2). This latter five-membered aromatic ring is a well known pharmacophore with remarkable biological properties,[25] and is representative of the numerous nitrogen-containing heterocycles found as hit fragments. Thus, the proposed synthetic pathway (Figure S3, Supporting Information) would allow the sequential introduction of the various scaffolds previously suggested. The aryl-aryl bond formation was performed by traditional palladium catalyzed Suzuki cross-coupling reaction. The introduction of the pyrrole or the imidazole was envisaged through *N*-arylation,[26,27] whereas the *C4*-imidazole analogue could be obtained in a single step. Thus, bi-aryl carboxamide derivatives (compounds **1a-e**, **2a-f**, **3a-d** and **4a-d**, Scheme 1A) were obtained by coupling adenine with commercially available biphenyl carboxylic acid **5a**, carbonyl chlorides **5b-e** or substituted biphenyl carboxylic acids **6a-f**, **7a-d** and **8a-d**. For the carboxylic acids coupling step, an excess of *N*,*N'*-carbonyldiimidazole (CDI) was used as activation reagent in presence of a catalytic amount of 4-dimethylaminopyridine (DMAP) in anhydrous DMF at 100 °C until starting material was consumed (HPLC monitoring). In the case of the imidazole derivatives **8a-d**, these coupling conditions led to simultaneous loss of the monomethoxytrityl (MMTr) protecting group. Substituted biphenyl carboxylic acids **6a-f** (Scheme 1B), **7a-d** and **8a-d** (Scheme 2) were obtained beforehand using Suzuki coupling of the corresponding boronic acid pinacol esters **11a,b** or commercially available boronic acid ethyl esters with substituted aryl bromides or derivatives **13a,b** and **17a,b**.

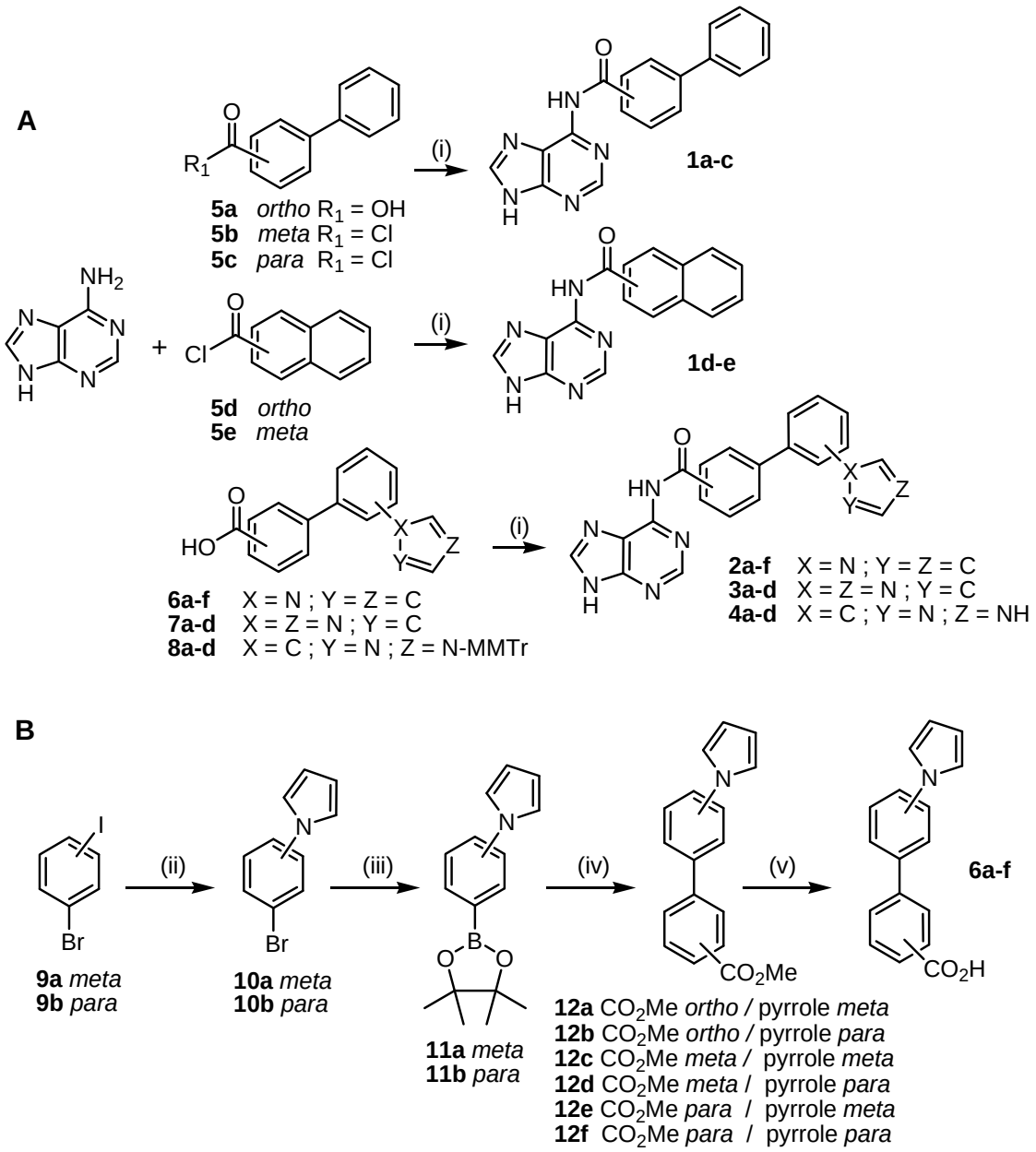

Scheme 1. Synthesis of targeted derivatives **1a-e**, **2a-f**, **3a-d** and **4a-d** (A) and intermediates **6a-f** (B). Reagents and conditions: (i) CDI, DMAP, DMF, 100 °C, 39 h-6.6 days (for R_1 = OH); or pyridine, 100 °C, 3 h (for R_1 = Cl); (ii) pyrrole, CuCl (5 mol%), *n*Bu_4NOH (40% aq.), 80 °C, 36 h; (iii) bis(pinacolato)diboron, $Pd_2(dba)_3$, 2-(dicyclohexylphosphino)-2',4',6'-triisopropylbiphenyl, AcOK,

DMF, 110 °C, 2 h; (iv) methylbromobenzoate, $Pd_2(dba)_3$, K_2CO_3, DMF, 100 °C, 18 h; (v) NaOH 2M, MeOH, 1,4-dioxane, 50 °C, 1-4 h (for **12a**-**e**); *t*-BuOK, Et_2O, H_2O, rt, 3 h (for **12f**).

The conditions described by Buchwald and co-workers,[28,29] were applied using potassium carbonate as base and tris(dibenzylideneacetone)dipalladium or tetrakis(triphenylphosphine) palladium as catalyst. A final treatment with aqueous NaOH in ethanol led to the saponification of the ester functions. For compounds containing the *C4*-imidazole heterocycle (Scheme 2), the nitrogen atom in position 1 of the 4-(bromophenyl)-1H-imidazole derivatives **16a** and **16b** was protected with a momomethoxytrityl group, leading in 96-98% yields to derivatives **17a** and **17b**, respectively. In contrast to the 4-(4-bromophenyl)-1*H*-imidazole **16b** which is commercially available, the imidazole moiety in meta position of compound **16a** was constructed from α-bromophenone derivative **15** treated by formamide according to an adapted procedure from the literature.[30,31]

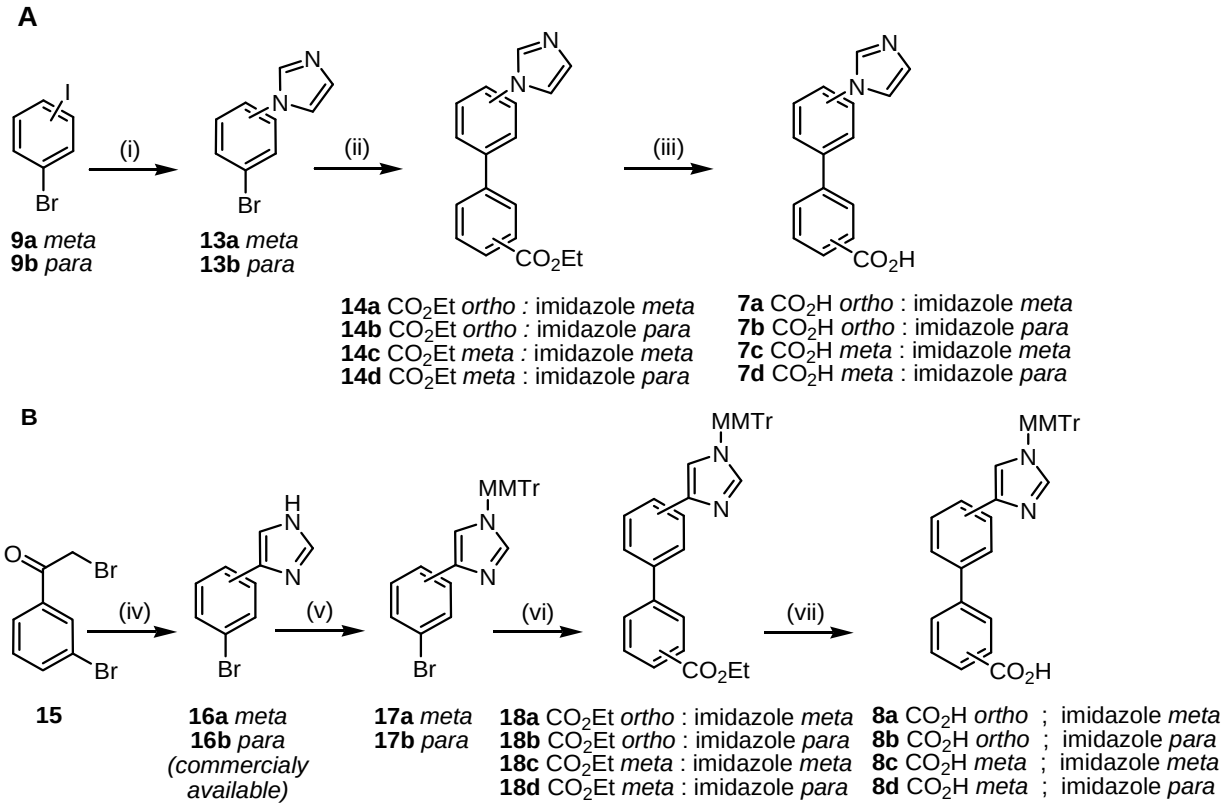

Scheme 2. Synthesis of intermediates **7a-d** and **8a-d** containing imidazole as heterocycle. Reagents and conditions: (i) Imidazole, CuI (10 mol%), benzotriazole (20 mol%), *t*-BuOK, DMSO, 100 °C, 14 h; (ii) ethoxycarbonylbenzeneboronic acid, $Pd(PPh_3)_4$, K_2CO_3, DMF, 100°C, 3-5 h; (iii) NaOH 2M, EtOH, 1,4-dioxane, 50 °C, 2-6 h; (iv) NH_2CHO, 170 °C, 14 h; (v) 4-monomethoxytrityl chloride, Et_3N, DMF, rt, 2 h; (vi) ethoxycarbonylbenzeneboronic acid, $Pd(PPh_3)_4$, K_2CO_3, DMF, 100 °C, 2-3 h; (vii) NaOH 2M, EtOH, 1,4-dioxane, 50 °C, 1-10 h.

cN-II inhibition by newly synthesized compounds

The chemical diversity obtained by using innovative synthesis pathways allowed us to evaluate most of the possible assemblies according to before-mentioned criteria. All new compounds were evaluated for their capacity to inhibit nucleotidase activity using the rapid green malachite

assay (Table 2). Interestingly, as soon as two fragments were linked together (bi-aryl and purine moieties) a strong inhibition was observed such as for the *meta*-compound **1b** with 68% at 0.2 mM. This result is in agreement with the docking prediction and the STD spectrum of this compound (Figure S4, Supporting Information). Indeed, compound **1b** was found to be deeply inserted into the IMP binding site and this prediction was confirmed by STD data showing that aromatic protons of the second phenyl are more buried (protons at position C2', C4' and C6'). The relative orientation of the second phenyl ring was found to be decisive as compound **1a** (*ortho*) was almost inactive at this concentration (17% inhibition) while *para* (**1c**) position was more advantageous with 57% inhibition. The effect of the addition of a third group (either pyrrole or imidazole) was also dependent on the orientation related to the second phenyl ring. As some compounds showed inhibitory activity after addition of the pyrrole group in positions *meta* (**2a**, 73% inhibition) and *para* (**2b**, 85% inhibition) whereas the corresponding unsubstituted compound was inactive (**1a**, phenyl in *ortho*). In contrast, when the second phenyl ring was oriented in *meta* or *para* position, the addition of either *N*-pyrrole or *N-/C4*-imidazole did not improve the efficacy of the final compound when compared to compound **1b** (assembly of two fragments), except for derivative **2c** which inhibited 56% of the cN-II activity. Compound **2f**, for which the orientation of phenyl and pyrrole rings is in *para/para,* was depicted as the less efficient compound with no activity detected at 0.2 mM. This result may indicate the limited space or volume available in the enzyme binding site as this particular derivative may be viewed as an extended scaffold. For *N*- or *C4*-imidazole-derived compounds (**3a-d** and **4a-d**), most of them were found to be inactive or weak inhibitors against cN-II (**3c**, **4a**, **4c** and **4d** with 39%, 35%, 25% and 26% inhibition, respectively). This result was surprising

according to the high structural similarity between imidazole and pyrrole. However, these two five-membered nitrogen-containing heterocycles share common features but differ in water solubility and acidity (pKa). Focusing on the most active compounds, the inhibition was further confirmed by steady state kinetics (Figure 4). Inhibition constants (K_i) were only determined for soluble compounds and were in agreement with the inhibition values observed at low concentration (0.2 mM). Inhibition constants ranged from 0.5 mM for **2b** to 2.8 mM for **1c** and are promising for further lead optimization, as previously identified competitive inhibitors showed higher K_i (≥ 1-2 mM). While the compounds based on a two-fragment assembly (**1b** and **1c**) were characterized as competitive inhibitors, derivatives based on the three-fragment assembly (**2a-c**) exhibited a non-competitive inhibition mode. The most potent compound (**2b**), with a K_i value of 0.46 mM, displayed a typical non-competitive inhibition kinetic. To illustrate such difference in inhibition mode, the kinetics of compounds **1b**, **2a** and **2b** are presented in Figure 4 with secondary and double-reciprocal plots. The initial prediction was carried out assuming that IMP was the targeted binding site for these inhibitors. However, structural analogies between this site and the regulatory sites (also binding nucleotides) may be responsible of this selection of alternative binding sites for compounds **2a-c**.

Table 2: Structures and inhibitory activities of bi-aryl carboxamide-N-(9*H*-purin-6-yl) derivatives (AdiS, a previously identified compound is shown as positive control).

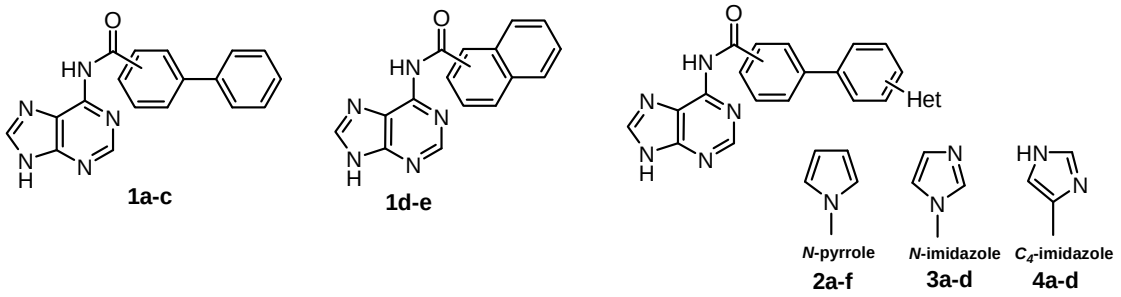

Compound #	Adenine / orientation	Substituent / orientation	Inhibition (%) at 0.2 mM	K_i (mM) (Inhibition mode)*
AdiS	-	-	20 ± 2%	2 ± 0.2
1a	*ortho*	-	17 ± 1%	n.d.**
1b	*meta*	-	68 ± 5%	0.95 ± 0.17 (Competitive)
1c	*para*	-	57 ± 3%	2.78 ± 0.61 (Competitive)
1d	*ortho*	-	40 ± 5%	n.d.
1e	*meta*	-	30 ± 5%	n.d.
2a	*ortho*	*N*-pyrrole / *meta*	73 ± 5%	1.65 ± 0.10 (Non-competitive)
2b	*ortho*	*N*-pyrrole / *para*	85 ± 4%	0.46 ± 0.03 (Non-competitive)
2c	*meta*	*N*-pyrrole / *meta*	56 ± 13%	0.79 ± 0.05 (Non-competitive)
2d	*meta*	*N*-pyrrole / *para*	28 ± 1%	n.d.
2e	*para*	*N*-pyrrole / *meta*	0%	n.d.

2f	*para*	*N*-pyrrole / *para*	0%	n.s.***
3a	*ortho*	*N*-imidazole / *meta*	13 ± 3%	n.d.
3b	*ortho*	*N*-imidazole / *para*	0%	n.s.
3c	*meta*	*N*-imidazole / *meta*	39 ± 7%	n.d.
3d	*meta*	*N*-imidazole / *para*	8 ± 8%	n.s.
4a	*ortho*	C_4-imidazole / *meta*	35 ± 5%	n.d.
4b	*ortho*	C_4-imidazole / *para*	3 ± 3%	n.d.
4c	*meta*	C_4-imidazole / *meta*	25 ± 5%	n.s.
4d	*meta*	C_4-imidazole / *para*	26 ± 5%	n.s.

*Values of inhibition and K_i are means from three independent experiments at different inhibitor concentrations ± SD. **n.d., not determined. ***n.s., not soluble at concentrations above 0.2 mM)

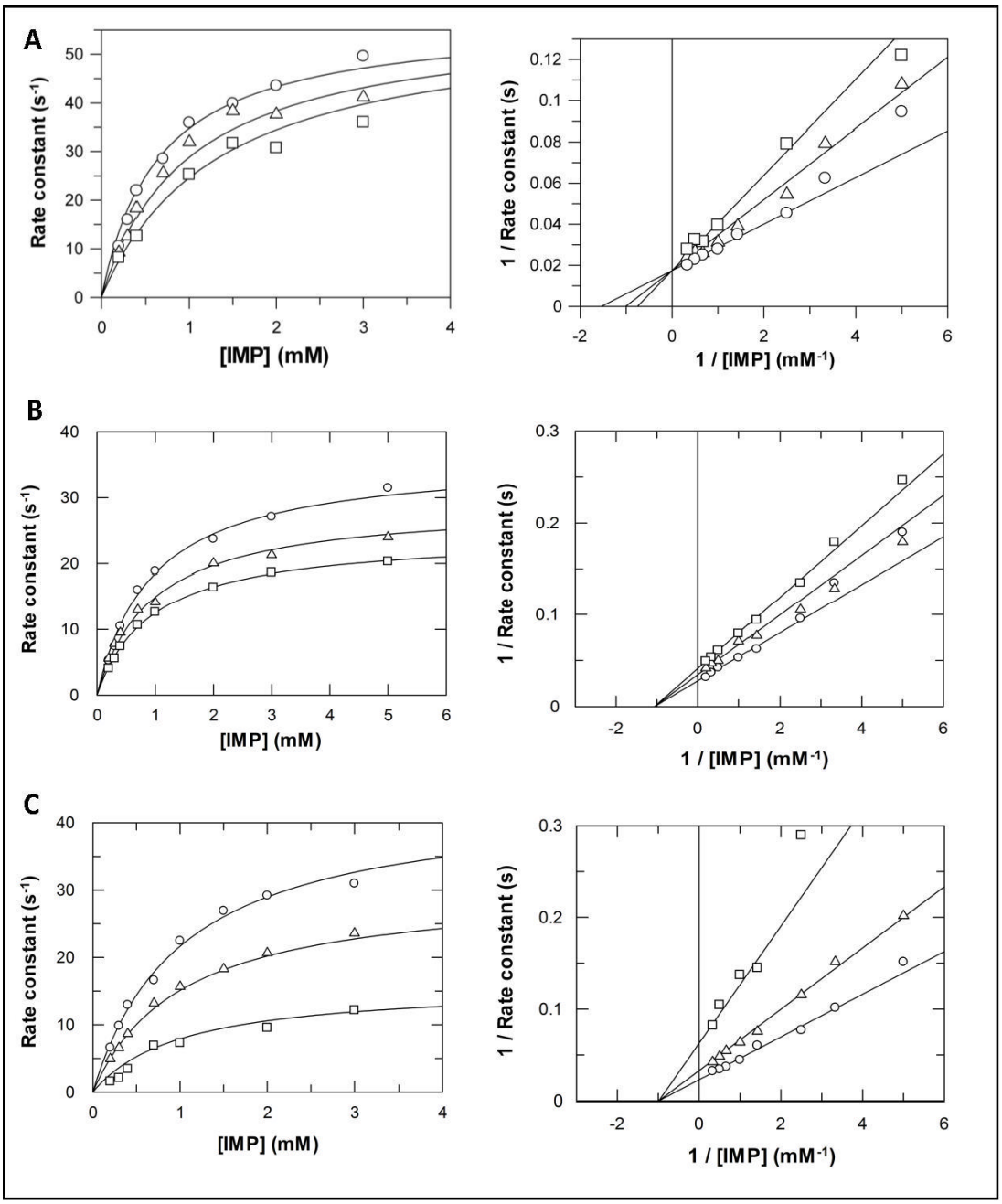

Figure 4: Secondary plots and double reciprocal representations of steady state rate constants as a function of substrate concentrations (IMP), for the most interesting compounds. (A) in the absence (○) or with **1b** at 0.5 mM (△) or 1 mM (□). (B) in the absence (○) or in the presence

of **2a** at 0.4 mM (△) or 0.8 mM (□). (C) in the absence (○) or in the presence of **2b** at 0.2 mM (△) or 0.8 mM (□).

Biological evaluation of newly synthesized compounds

All derivatives were evaluated for their antiproliferative activity on cancer cells. IC_{50} values as determined by the MTT assay on human follicular lymphoma cells (RL) ranged from 4.7 to 215 µM (Table 3). For compounds with IC_{50} lower than 100 µM, their synergistic activities with nucleoside analogues were evaluated. This is based on the assumption that cN-II inhibitors should act synergistically with cytotoxic nucleoside analogues as was shown with inhibitors issued from virtual screening and by sensitization of cancer cells with low expression of cN-II.[24,32,33] Synergy was observed with several combinations with cladribine and clofarabine as for example compound **1b** (CI95 = 0.8 and 0.8), compound **2d** (CI95 = 0.8 and 0.7), compound **2f** (CI95 = 0.5 and 0.7), compound **3c** (CI95 = 0.8 and 0.7) and compound **4c** (CI95 = 0.9 and 0.6). However, no synergy was detected with fludarabine (compound **2d** being excepted with the limit value of 0.9), suggesting a distinct metabolism for this compound. This difference with fludarabine was also observed with AdiS, a first-generation cN-II inhibitor identified by virtual screening.[24]

Table 3: Biological activity of the newly synthesized compounds on RL cells. IC_{50} values (µM) and CI95 values are mean values of at least three independent experiments ± SEM. Compounds for

which IC_{50} value was below 100 µM are highlighted in light grey and their synergistic activities in dark grey (AdiS is a previously identified compound by virtual screening).

Compound # / IC_{50}		CI95 Fludarabine	CI95 Cladribine	CI95 Clofarabine
AdiS	1036 ± 267	4.2 ± 1.7	0.4 ± 0.1	0.24 ±.0.03
1a	165 ± 41	n.d.	1.1 ± 0.2	n.d.
1b	25 ± 4	1.2 ± 0.2	0.8 ± 0.1	0.8 ± 0.1
1c	157 ± 38	n.d.	n.d.	n.d.
1d	>300	n.d.	n.d.	n.d.
1e	240 ± 31	n.d.	n.d.	n.d.
2a	23 ± 9	n.d.	1.2 ± 0.8	n.d.
2b	35 ± 3	1.5 ± 0.2	1.4 ± 0.1	1.0 ± 0.1
2c	11 ± 2	1.4 ± 0.3	1.4 ± 0.2	2.9 ± 1.3
2d	8 ± 2	0.9 ± 0.1	0.8 ± 0.1	0.7 ± 0.2
2e	398 ± 62	n.d.	n.d.	n.d.
2f	87 ± 22	1.3 ± 0.3	0.5 ± 0.2	0.7 ± 0.1
3a	168 ± 32	n.d.	n.d.	n.d.
3b	51 ± 9	1.1 ± 0.1	1.2 ± 0.2	1.8 ± 1.0
3c	34 ± 5	1.9 ± 0.8	0.8 ± 0.2	0.7 ± 0.2
3d	203 ± 20	n.d.	n.d.	n.d.
4a	215 ± 8	n.d.	n.d.	n.d.
4b	107 ± 3	n.d.	n.d.	n.d.

4c	30 ± 3	2.9 ± 1.7	0.9 ± 0.2	0.6 ± 0.3
4d	5 ± 1	3.7 ± 2.5	1.2 ± 0.3	0.4 ± 0.2

Binding sites of two active FBDD assemblies

For the inhibitors which displayed highest biology activity on RL cells (see Table 3) and which were water-soluble (**1b**, **2c**, **3c** and **4c)**, co-crystallization and soaking experiments were performed. Crystals grew in the presence of ligands **2c** and **3c**, and the crystal structure, hereof a new form crystallizing under conditions never reported so far for the complex with ligand **2c** (Table S1, Supporting Information), displays an overall same fold as those previously reported,[24,34] with an α/β core-domain and a cap-domain (Figure 5A). The two complexes display an RMSD of 0.88 Å (**2c**) and 0.78 Å (**3c**) compared to PDB-ID 2J2C, respectively. Two molecules are present in the asymmetric unit for both ligand complexes, for which electron density in chain A is visible for residues 26-493 with both compounds, but with two disordered helix regions (317-321 and 357-360) for **2c** and a short chain break (357-358) for **3c**. As concerns chain B, electron density is visible for residues 26-493 (**2c**) and 26-492 (**3c**), with disordered regions being 314-324, 359-361 (**2c**) and 315-322, 357-362 (**3c**). As seen in Figure 5B (with ligand **2c**), an important amount of domain swapping is observed for these protein complexes. This particular feature suggests a strong influence of the ligand binding on the structural organization of the enzyme. Analysis of the dimer interfaces between molecules A and B in the two structures employing the PISA online server,[35] revealed the presence of 39/35 hydrogen bonds and 9/10 salt-bridge interactions at the subunit interface for cN-II structures with ligands **2c**/**3c**, respectively.

Interestingly, a region reported disordered (401-416) in the previously determined structures,[24,34,36] due to flexibility, is visible and well ordered in the two structures with ligands **2c** and **3c**, as is an additional part of the C-terminal (Figure 5C). The position of **2c** in the structure is unique and has not been observed in previous solved structures (Figure 5C and D). Indeed the ligand is stacked between α-helices formed by residues 228-240 and 371-401 in a cleft in the α/β core-domain at the back of the active site, at a distance of ~10 Å of this latter, where the N-pyrrole part of ligand **2c** is positioned at the place of helix α1 from the apo-structure (2XCX,[36]). When comparing the apo- and ligand bound structures, the long α-helix formed by residues 376-401 displays a kink at residue 383, and the last part of the helix (383-401) has been tilted by 15°. In molecule A, electron density corresponding to the entire ligand was clearly present, whereas in chain B only the electron density corresponding to the adenosine moiety was clearly visible. For this reason, in molecule B only the adenosine moiety was refined in the structure. In both molecules interactions between ligand **2c** and the enzyme are made *via* hydrogen-bonds (S464) and hydrophobic (V59, V227, I466) interactions or *via* water molecules (D229, A463) to the adenosine part of the ligand. The position of **3c** in the structure has not been observed in earlier solved structures (Figure 5E). Indeed, electron densities clearly indicated that two molecules of **3c** are stacked between two cap domains at the dimer interface where parts of the N- and C-termini join. The ligand interacts with residues S40, L476 and R478 from molecule A and with residues Q420, S445 and R446 from molecule B (Figure 5F).

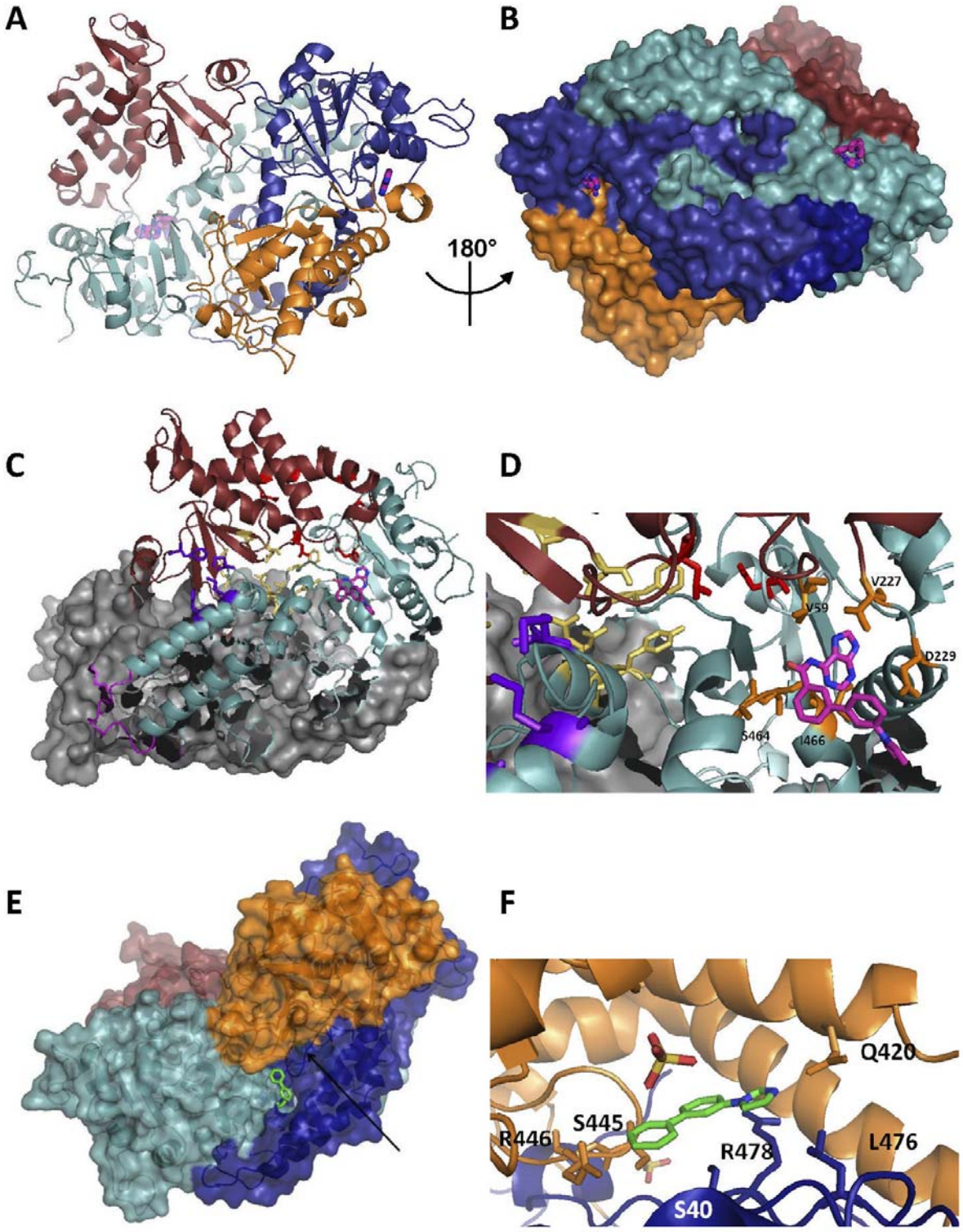
A
B
180°
C
D
V227
V59
D229
S464
I466
E
F
Q420
S445
R446
R478
L476
S40

Figure 5: (A) Dimer structure in the cN-II-**2c** complex. For molecule A the cap-domain is shown in light-cyan and the core-domain in brown, whereas for molecule B these are shown in dark-blue and orange, respectively. Ligand **2c** (pink) is binding to the cap-domain in both molecules but only one was fully visible. **(B)** Surface presentation of the cN-II-**2c** complex displaying domain swapping between dimers, and binding cavities for ligand **2c**. Color codes are as in panel (A). **(C)** cN-II-**2c** complex in a secondary structure presentation showing molecule A, and molecule B as a surface presentation. Color codes are as in panel (A), with the active site region in red, effector site 1 in yellow and effector site 2 in purple. The region corresponding to the loop which has not been observed in any previously solved crystal structure of cN-II as well as ligand **2c** are shown in pink, and the C-terminal part of the molecule is displayed in dark blue and **(D)** Close-up view of the newly identified binding site of ligand **2c** in which interacting residues are highlighted in orange. **(E)** Surface presentation of the cN-II-**3c** complex displaying domain swapping between dimers, and ligand binding cavities with ligand **3c** binding at the interface of molecules A and B. The arrow indicates the binding site of the second ligand **3c** molecule and color codes are as in panel (a). **(F)** Close-up on the **3c** ligand binding site at the interface of molecules A and B.

DISCUSSION AND CONCLUSIONS

Using a small library of 300 fragments and targeting a particularly difficult enzyme, two sub-groups of fragments were identified by NMR studies and most of them were able to inhibit nucleotidase activity of cN-II. Molecular docking studies guided the merging process and the *in*

vitro evaluation of two more compounds (**F15** and **F16**) gave additional experimental evidences of the relevance of our approach. Thus, the synthesis of 19 novel compounds was achieved in order to enhance the success rate as the degree of freedom increases with the size of the molecule. However, negative results can appear as for compounds **1d** and **1e** that turned out to be no better than the initial fragment, *i.e.* the naphthyl moiety (40% of inhibition for both fragment **F9** and compound **1d**). Interestingly, we noticed that when two fragments were combined (for instance, compounds **1a** to **1e**), the orientation of the second one (bi-aryl or naphthyl) was highly sensitive and governed the inhibition efficiency (when comparing compounds **1a** and **1b**, for instance). With the two-fragment assemblies, a competitive inhibition mode was observed against cN-II activity. This result was expected according to the INPHARMA and docking results obtained earlier. However and surprisingly, enlarging the size of the compounds (*i.e.* the association of three fragments) resulted in a change of the inhibition mode (as shown with compounds **2a**, **2b** and **2c**). Although the initial strategy was targeting the active site, the discovery of more potent and non-competitive inhibitors is highly encouraging. Definitely, such inhibitors may behave more selective and cannot be displaced by a high substrate concentration as competitive inhibitors.

Five compounds were found to be cytotoxic when tested on cancer cell lines (RL) as shown by their IC_{50} values in the low micromolar range. Although this result is very promising, one may speculate about the specificity of the observed inhibition. In order to get further insights, synergy experiments were performed in presence of well-known cytotoxic nucleoside analogues used in anticancerous therapies. Several molecules (**1b**, **2d**, **2f**, **3c** and **4c**) that induced an antiproliferative activity on cancer cells were also linked to a synergistic effect,

mainly with clofarabine and cladribine but not with fludarabine. Clarifying the absence of synergy with fludarabine is complex since fludarabine monophosphate is a substrate of cN-II,[37] and fludarabine was recently described as a mixed cN-II inhibitor through its binding to the active site and a regulatory site.[21] Moreover, a recent publication showed that human glioblastoma cells with decreased expression of cN-II were resistant to fludarabine.[32] This clearly indicates a different metabolism of fludarabine as compared to clofarabine and cladribine and consequently disfavoring the synergistic effect. Nevertheless, a synergy was observed with some compounds indicating that the inhibition of cN-II is beneficial for the metabolism of these two cytotoxic nucleoside analogs. Our results also pointed out the non-selectivity of one derivative (**2f**) which did not inhibit the cN-II activity *in vitro* but promoted a synergy with cladribine and clofarabine. The discrepancy observed between the *in vitro* inhibitory activity and antiproliferative effects of some compounds may be explained by the low target specificity for few compounds in a cell context, as shown by the low IC_{50} values and may also be due to their poor water-solubility leading to a weak cellular uptake (loss of compound in membrane compartments). When synergy is observed for a compound without detecting any cN-II inhibition, this clearly denotes the presence of another target, likely another enzyme in charge of the anticancerous drug metabolism or activation.

Therefore, to better understand the mechanism by which our compounds actually alter the enzyme activity, X-ray crystallography was successfully achieved with two of them (**2c** and **3c**). As indicated in the results section, the ligand **2c** occupies the position of α-helix 1 in the apo-enzyme structure. This position constitutes a new binding site that was not previously identified, and underlines the highly dynamic system observed for this regulatory enzyme. The

binding of ligand **2c** may induce dramatic changes in the functional dynamics of the enzyme and may explain the non-competitive inhibition mode observed in kinetics. Inspection of the crystal structure of cN-II-**3c**, indicated that ligand **3c** also bound to a previously unidentified binding site located at the dimer interface between the cap domains. Thus, one may speculate that the effect of ligand **3c** is due to a perturbation of the "gathering point" at this interface and thereby may potentially affect the oligomerization state of the enzyme. Indeed, both enzyme complexes display a new crystal form in which a dimer is formed *via* domain swapping, a feature which has been reported for other systems as being essential for oligomer assembly.[38,39] Therefore, oligomerization and thereby domain swapping of this enzyme putatively is highly physiologically relevant and may be involved in the enzyme activity or regulation. Interestingly, both ligand compounds in the solved structure differ in terms of inhibition efficiency as **2c** was found more active *in vitro* without any synergy on cell models and **3c** was less active *in vitro* but with synergy on cell models. The chemical structure of both compounds is highly similar especially in the orientation of the phenyl and imidazole or pyrrole groups (meta/meta orientation in each case). According to the *in vitro* and *in cellulo* data, it appears advantageous for these inhibitors to incorporate a pyrrole group instead of an imidazole. Interestingly, structurally similar fragments (bi-aryl, naphthyl and pyrrole) were found in the search of inhibitors against an analogous enzyme, the human purple acid phosphatase.[13,40] In this case, naphthalene derivatives (inactive against cN-II) were active in the low micromolar range indicating that although these enzymes share common structural features, they differ in their active site and enzymatic reaction mechanism. The inhibition constants determined for the most active compounds are still in the low millimolar range, that is insufficient for drug development and the next challenging step will

concern the optimization of these compounds. Several structure-based (QSAR) or ligand-based (pharmacophore models and scaffold hoping) strategies may be employed to improve the efficiency of these cN-II inhibitors.

Even though further investigations and lead optimization are still needed to bring farther these compounds up to their clinical use, the discovery of new potent drug candidates constitutes a promising result for their future application in combined therapies with cytotoxic nucleoside analogues and the treatment of hematological malignancies.

EXPERIMENTAL SECTION

NMR screening: The chemical library consisted of 300 fragments with molecular weights below 300 g/mol.[41]. The average molecular weight is 170 g/mol and all compounds were checked for their solubility in aqueous buffer at 1 mM. Average calculated logP was estimated to be 1.27. NMR screening was carried out on the N-terminal truncated cN-II using a 600 MHz NMR in the presence of fragments (600 µM) either in 50 mM potassium phosphate buffer pH 7.0, 500 mM NaCl or in 50 mM imidazole pH 6.5, 500 mM NaCl at 20 °C. 1D 1H Saturation Transfer Difference (STD) and Waterlogsy experiments were performed on samples containing mixtures of 5 fragments preselected not to interfere with each other. Saturation time for the STD experiment was 2s and mixing time for the Waterlogsy experiment set to 1.5 s. All the hits identified were further validated by recording the same experiments with the fragments one by one. The STD factor value F_{STD} was calculated as $I_{STD}/I_0*L_{TOT}/P_{TOT}$, where I_{STD} and I_0 are the peak integrals for the STD and STD_{off} experiments, and L_{TOT} and P_{TOT} the total concentrations of the ligand and

protein, respectively. The errors in F_{STD} calculation is estimated to 10%. For the assessment of the solvent accessibility, F_{STD} values were calculated for each proton, then values were normalized. The highest value was set to 100%. NOESY experiments for the INPHARMA experiments were performed in the presence of cN-II (20 µM) and 1 mM of two ligands, with a mixing time of 300 ms.

Docking of fragments: Molecular docking was performed using Gold 5.1 program (Genetic Optimization for Ligand Docking, CCDC Software Limited) by applying 50 genetic algorithm runs in the IMP binding site of the human cN-II three-dimensional structure (2XCW). Magnesium ion and crystal water molecules (involved in the catalysis) were preserved and Mg^{2+} was selected as target atom to define the docking site forming a spherical area with a radius of 15 Å. Docking poses were classified according to their respective score calculated by the Goldscore scoring function. The different docking poses were analyzed by the clustering method (complete linkage) from the rmsd matrix of ranking solutions. The structural analysis and visualization of docking poses was carried out using the Pymol software (The PyMOL Molecular Graphics System, Version 1.3 Schrödinger, LLC).

Protein expression and purification: For *in vitro* studies, the N-terminal truncated cN-II,[42] was produced in *E. coli* according to the procedure previously described.[19,20] To control that the N-terminal deletion was harmless, the full-length cN-II (FL) was also cloned into a pET28a plasmid and produced similarly (full details are presented in *SI Experimental procedures*).

Nucleotidase activity assays: The nucleotidase activity was measured using the Green Malachite Phosphate Assay Kit (Gentaur) as previously described.[19] For non-water soluble

fragments, DMSO was used and the final percentage in the assay did not exceed 2% in order to preserve the enzyme activity.

Steady state kinetics assay: The kinetic parameters including Michaelis-Menten, rate and inhibition constants were obtained from steady state kinetics. This method was used to determine the inhibition mode and K_i values for the most interesting compounds. Hence, the recombinant purified enzyme (0.1 µm) and substrate (IMP at different concentration varying from 200 µM to 3 mM) freshly prepared in the same buffer as above (nucleotidase assay) were mixed together in a thermostatically controlled beaker under magnetic stirring at 37 °C. The reaction was stopped at different times by adding 10% of perchloric acid. The typical time course duration was 35 s with a sampling frequency every 7 s. Quantification of IMP and inosine content present in the quenched reaction mixture was performed by HPLC (Waters Alliance) using a Partisphere 5-SAX column (Whatman) and 10 mM ammonium phosphate buffer pH 5.5 as mobile phase. The raw data were analyzed using Grafit 7 (Erithacus Software) and fitted with an equation describing either a competitive, non-competitive or mixed inhibition mode in order to determine the mode and associated K_i values. Competitive inhibitions (describing inhibition curves for compounds **1b** and **1c**) were fitted using the equation (1) while non-competitive inhibitions (compounds **2a-c**) were fitted with equation (2).

$$v = \frac{V_{Max}\,[S]}{[S] + K_M\left(1+\frac{I}{K_i}\right)} \qquad (1) \qquad\qquad v = \frac{V_{Max}[S]\cdot\frac{1}{1+[I]/K_i}}{[S] + K_M} \qquad (2)$$

Crystallization, data reduction, structure determination and refinement: Crystallization experiments were performed using the sitting drop vapor diffusion method. Freshly purified protein was mixed with ligands **2c** and **3c** and incubated at 4 °C for 20 mins. Crystals appeared

after one week at 4 °C and diffraction data were collected at the European Synchrotron radiation facility (ESRF Grenoble France). Coordinates and structure factors of the cN-II complexes have been deposited at the RCSB under the entry codes 5CR7 and 5CQZ for cN-II-**2c** and cN-II-**3c**, respectively. Coordinates and structure factors of the cN-II complexes have been deposited at the RCSB (Research Collaboratory for Structural Bioinformatics) Protein Data Bank (http://www.rcsb.org) under the entry codes 5CR7 and 5CQZ for cN-II-**2c** and cN-II-**3c**, respectively (more details are presented in Supporting Information, Experimental procedures).

Cytotoxicity assay and evaluation of synergy: The cytotoxicity of assembled fragments alone or in combination with nucleoside analogues (cladribine, clofarabine and fludarabine) was evaluated on RL cells with a MTT assay (Sigma) as described earlier.[24] For evaluation of synergy between assembled fragments and nucleoside analogues, RL cells were seeded in 96 well plates containing varying concentrations of assembled fragments alone, nucleoside analogue alone or a mixture of assembled fragments and nucleoside analogue at constant ratios that were slightly higher or lower than the ratio IC_{50}drug / IC_{50}inhibitor. After incubation for 72 hours, living cells were quantified with the MTT assay. Values for inhibitory concentration 50 (IC_{50}) and combination index 95 (CI_{95}) were calculated with CompuSyn software 1.0 (ComboSyn, Inc., USA). Synergy was defined as $CI_{95} < 0.9$, additivity as $0.9 < CI_{95} < 1.1$ and antagonism as $CI_{95} > 1.1$.[43]

Chemistry

General Methods: All moisture sensitive reactions were carried out under rigorous anhydrous conditions with argon atmosphere and using oven-dried glassware. Solvents were dried and distilled prior to use, and solids were dried over P_2O_5 under reduced pressure. ^{1}H NMR and ^{13}C

NMR spectra were recorded at ambient temperature on a Bruker 300 Avance or DRX 400. Chemical shifts (δ) are quoted in parts per million (ppm) referenced to the residual solvent peak, ($CDCl_3$ fixed at 7.26 and 77.16 ppm, DMSO-d6 fixed at 2.50 and 39.52 ppm) relative to tetramethylsilane (TMS). Deuterium exchange and COSY experiments were performed in order to confirm proton assignments. Coupling constants, *J*, are reported in hertz. 2D $^{1}H–^{13}C$ heteronuclear COSY was recorded for the attribution of ^{13}C signals when needed. ESI mass and high resolution mass spectra were recorded in the positive or negative-ion mode on a Micromass Q-TOF. Thin-layer chromatography was performed on precoated aluminum sheets of Silica 60 F254 (Merck, Art. 5554), visualization of products being accomplished by UV absorbance. Chromatography was performed on Merck Silica Gel 60 (230−400 mesh ASTM). Analytical HPLC chromatograms were obtained using a Waters HPLC system (separation module 2695, 996 photodiode array detector 2996) and a Waters Symmetry Shield (50 mm × 4.6 mm, 3.5 µm) RP-18-column with a 1 mL/min flow rate. The elution solvents were water containing 0.1% (v/v) of TFA (solvent A) and acetonitrile containing 0.1% (v/v) TFA (solvent B). A linear gradient was performed from 100% of solvent A to 100% of solvent B in 7 or 15 min. All tested compounds were confirmed to have ≥95% purity, determined by HPLC.

General procedure for the synthesis of compounds 1a, 2a-f, 3a-d and 4a-d

To a stirred solution of adenine (3.03 mmol) in DMF (15 mL) was added under argon the corresponding carboxylic acid **5a**, **6a-f**, **7a-d** or **8a-d** (1.51 mmol), *N*,*N*'-carbonyldiimidazole (3.03 mmol) and *N*,*N*-dimethyl-4-aminopyridine (0.30 mmol). The reaction mixture was stirred at 100°C until HPLC revealed that the starting material was consumed. Solvent were removed

under reduced pressure and the residue was purified on silica gel column chromatography (dichloromethane/MeOH, 0-10%) to provide compounds **1a, 2a-f, 3a-d** and **4a-d.**

***2-Phenyl-N-(9H-purin-6-yl)benzamide* (1a):** yield = 19%; white powder; ^{1}H NMR (DMSO-d_6): δ = 7.24-7.36 (m, 3H), 7.46-7.54 (m, 4H), 7.60-7.65 (m, 1H), 7.72 (d, 1H, ^{3}J = 6.0 Hz), 8.41 (s, 1H), 8.60 (s, 1H), 11.49 (bs, 1H), 12.16 (bs, 1H); ^{13}C NMR (DMSO-d_6): δ = 113.4, 127.2, 127.4, 128.3 (2C), 128.4 (2C), 128.6, 130.1, 130.7, 135.0, 139.9, 140.0, 144.0, 145.9, 151.2, 162.0, 169.3; MS (ESI) *m/z* 316.1 $[M+H]^+$; HRMS: calcd for $C_{18}H_{14}N_5O$ $[M+H]^+$ 316.1198, found 316.1201; HPLC t_R = 6.9 min, 100%.

***N-(9H-Purin-6-yl)-2-(3-pyrrol-1-ylphenyl)benzamide* (2a):** yield = 53%; white powder; ^{1}H NMR (DMSO-d_6): δ = 6.30 (t, 2H, ^{3}J = 2.0 Hz), 7.37 (t, 2H, ^{3}J = 2.0 Hz), 7.38-7.65 (m, 6H), 7.76 (d, 2H, ^{3}J = 8.0 Hz), 8.47 (s, 1H), 8.66 (s, 1H), 11.65 (bs, 2H); ^{13}C NMR (DMSO-d_6): δ = 110.6 (2C), 113.7, 118.4, 119.0 (2C), 119.4, 125.4, 127.6, 128.6, 129.7, 130.2, 130.8, 135.4, 139.3, 139.9, 141.4, 144.2, 145.8, 151.2, 161.4, 169.2; MS (ESI) *m/z* 381.2 $[M+H]^+$; HRMS: calcd for $C_{22}H_{17}N_6O$ $[M+H]^+$ 381.1464, found 381.1471; HPLC t_R = 7.9 min, 98.6%.

***N-(9H-Purin-6-yl)-2-(4-pyrrol-1-ylphenyl)benzamide* (2b):** yield = 13%; white powder; ^{1}H NMR ($CDCl_3$): δ = 6.34 (t, 2H, ^{3}J = 2.0 Hz), 7.08 (t, 2H, ^{3}J = 2.0 Hz), 7.39-7.51 (m, 6H), 7.65 (t, 1H, ^{3}J = 6.0 Hz), 7.75 (d, 1H, ^{3}J = 9.0 Hz), 8.25 (s, 1H), 8.31 (s, 1H), 9.25 (bs, 1H), 11.55 (bs, 1H); ^{13}C NMR ($CDCl_3$): δ = 111.2 (2C), 112.9, 119.2 (2C), 120.7 (2C), 128.3, 129.0, 130.0 (2C), 131.2, 132.4, 133.7, 136.4, 140.1, 140.8, 143.2, 144.5, 152.2, 162.9, 169.4; MS (ESI) *m/z* 381.2 $[M+H]^+$; HRMS: calcd for $C_{22}H_{17}N_6O$ $[M+H]^+$ 381.1464, found 381.1468; HPLC t_R = 7.4 min, 100%.

***N-(9H-Purin-6-yl)-3-(3-pyrrol-1-ylphenyl)benzamide* (2c):** yield = 75%; white powder; ^{1}H NMR (DMSO-d_6): δ = 6.33 (t, 2H, ^{3}J = 2.0 Hz), 7.54 (t, 2H, ^{3}J = 2.0 Hz), 7.57-7.76 (m, 4H), 8.02 (s, 1H), 8.13 (dd, 2H, ^{3}J = 8.0 Hz, ^{4}J = 2.0 Hz), 8.54 (s, 1H), 8.56 (s, 1H), 8.78 (s, 1H), 12.01 (bs, 2H); ^{13}C NMR (DMSO-d_6): δ = 110.6 (2C), 115.5, 118.0, 119.0, 119.4 (2C), 123.9, 127.1, 128.2, 129.4, 130.4, 131.2, 133.5, 139.7, 140.7, 140.9, 145.2, 146.0, 151.2, 161.4, 166.4; MS (ESI) *m/z* 381.0 $[M+H]^+$; HRMS: calcd for $C_{22}H_{17}N_6O$ $[M+H]^+$ 381.1464, found 381.1456; HPLC t_R = 9.1 min, 99.3%.

***N-(9H-Purin-6-yl)-3-(4-pyrrol-1-ylphenyl)benzamide* (2d)**: yield = 51%; white powder; ^{1}H NMR (DMSO-d_6): δ = 6.33 (t, 2H, ^{3}J = 2.0 Hz), 7.50 (t, 2H, ^{3}J = 2.0 Hz), 7.70 (t, 1H, ^{3}J = 8.0 Hz), 7.76 (d, 2H, ^{3}J = 8.0 Hz), 7.97 (d, 2H, ^{3}J = 8.0 Hz), 8.02-8.12 (m, 2H), 8.51 (s, 1H), 8.54 (s, 1H), 8.78 (s, 1H), 12.16 (bs, 2H); ^{13}C NMR (DMSO-d_6): δ = 110.7 (2C), 115.5, 119.0 (2C), 119.6 (2C), 126.5, 127.6, 128.1 (2C), 129.3, 130.6, 133.5, 135.9, 139.4, 139.6, 145.1, 145.8, 151.2, 160.9, 166.4; MS (ESI) *m/z* 381.1 $[M+H]^+$; HRMS: calcd for $C_{22}H_{17}N_6O$ $[M+H]^+$ 381.1464, found 381.1461; HPLC t_R = 9.1 min, 100%.

***N-(9H-Purin-6-yl)-4-(3-pyrrol-1-ylphenyl)benzamide* (2e):** yield = 50%; white powder; ^{1}H NMR (DMSO-d_6): δ = 6.30 (t, 2H, ^{3}J = 1.4 Hz), 7.52 (t, 2H, ^{3}J = 1.4 Hz), 7.58 (t, 1H, ^{3}J = 5.2 Hz), 7.63-7.66 (m, 2H), 7.94 (s, 1H), 8.01 (d, 2H, ^{3}J = 5.6 Hz), 8.24 (d, 2H, ^{3}J = 5.6 Hz), 8.52 (s, 1H), 8.75 (s, 1H), 12.12 (bs, 2H); ^{13}C NMR (DMSO-d_6): δ = 110.6 (2C), 114.6, 117.8, 119.3, 119.3 (2C), 123.9, 127.0 (2C), 129.3 (2C), 130.5, 132.0, 140.5, 140.7, 143.4, 145.1, 146.0, 151.2, 161.8, 166.2; MS (ESI) *m/z* 381.1 $[M+H]^+$; HRMS: calcd for $C_{22}H_{17}N_6O$ $[M+H]^+$ 381.1464, found 381.1453; HPLC t_R = 9.1 min, 100%.

***N-(9H-Purin-6-yl)-4-(4-pyrrol-1-ylphenyl)benzamide* (2f):** yield = 33%; light brown powder; ^{1}H NMR (DMSO-d_6): δ = 6.37 (t, 2H, ^{3}J = 1.4 Hz), 7.55 (t, 2H, ^{3}J = 1.4 Hz), 7.80 (d, 2H, ^{3}J = 8.0 Hz),

7.95-8.02 (m, 4H), 8.29 (d, 2H, ^3J = 8.0 Hz), 8.57 (s, 1H), 8.81 (s, 1H), 12.11 (bs, 2H); ^{13}C NMR (DMSO-d_6): δ = 110.7 (2C), 114.7, 118.9 (2C), 119.5 (2C), 126.2 (2C), 126.9, 128.1 (2C), 129.2 (2C), 131.5, 135.4, 139.8, 143.0, 145.6, 151.0, 161.1, 166.1; MS (ESI) *m/z* 381.1 $[M+H]^+$; HRMS: calcd for $C_{22}H_{17}N_6O$ $[M+H]^+$ 381.1464, found 381.1463; HPLC t_R = 9.1 min, 98.1%.

***2-(3-Imidazol-1-ylphenyl)-N-(9H-purin-6-yl)benzamide* (3a):** yield = 28%; white powder; ^{1}H NMR (DMSO-d_6): δ = 7.08 (s, 1H), 7.42-7.47 (m, 2H), 7.53-7.76 (m, 7H), 8.23 (s, 1H), 8.39 (s, 1H), 8.59 (s, 1H), 11.85 (bs, 2H); ^{13}C NMR (DMSO-d_6): δ = 115.2, 118.0, 119.3, 120.3, 127.0, 127.7, 128.7, 129.8, 129.9, 130.3, 130.8, 135.3, 135.5, 136.9, 139.0, 141.6, 144.7, 145.8, 151.1, 160.8, 169.1; MS (ESI) *m/z* 382.1 $[M+H]^+$; HRMS: calcd for $C_{21}H_{16}N_7O$ $[M+H]^+$ 382.1416, found 382.1426; HPLC t_R = 4.7 min, 100%.

***2-(4-Imidazol-1-ylphenyl)-N-(9H-purin-6-yl)benzamide* (3b):** yield = 20%; white powder; ^{1}H NMR (DMSO-d_6): δ = 7.08 (s, 1H), 7.52-7.59 (m, 4H), 7.63-7.66 (m, 3H), 7.73-7.76 (m, 2H), 8.24 (s, 1H), 8.40 (s, 1H), 8.61 (s, 1H), 11.67 (bs, 1H), 12.18 (bs, 1H); ^{13}C NMR (DMSO-d_6): δ = 115.3, 118.3, 120.5 (2C), 127.9, 129.3, 130.3 (2C), 130.4, 130.6, 131.3, 135.5, 135.9, 136.6, 138.9, 139.4, 145.0, 146.2, 151.6, 161.8, 169.6; MS (ESI) *m/z* 382.2 $[M+H]^+$; HRMS: calcd for $C_{21}H_{16}N_7O$ $[M+H]^+$ 382.1416, found 382.1417; HPLC t_R = 4.7 min, 100%.

***3-(3-Imidazol-1-ylphenyl)-N-(9H-purin-6-yl)benzamide* (3c):** yield = 43%; white powder; ^{1}H NMR (DMSO-d_6): δ = 7.15 (s, 1H), 7.62-7.75 (m, 3H), 7.83-7.89 (m, 2H), 8.10-8.14 (m, 3H), 8.40 (s, 1H), 8.52 (s,1H), 8.55 (s, 1H), 8.76 (s, 1H), 12.09 (bs, 2H); ^{13}C NMR (DMSO-d_6): δ = 114.8, 118.3, 119.0, 119.9, 125.4, 127.1, 128.3, 129.4, 129.9, 130.5, 131.2, 133.5, 135.8, 137.7, 139.3, 141.0, 144.8, 146.0, 151.2, 162.2, 166.3; MS (ESI) *m/z* 382.2 $[M+H]^+$; HRMS: calcd for $C_{21}H_{16}N_7O$ $[M+H]^+$ 382.1416, found 382.1418; HPLC t_R = 5.4 min, 98.5%.

***3-(4-Imidazol-1-ylphenyl)-N-(9H-purin-6-yl)benzamide* (3d):** yield = 14%; white powder; ^{1}H NMR (DMSO-d_6): δ = 7.15 (s, 1H), 7.70 (t, 1H, ^{3}J = 6.0 Hz), 7.81-7.85 (m, 3H), 7.92-8.13 (m, 4H), 8.37 (s, 1H), 8.52 (s, 2H), 8.76 (s, 1H), 11.77 (bs, 1H), 12.41 (bs, 1H); ^{13}C NMR (DMSO-d_6): δ = 115.2, 118.4, 121.1(2C), 127.1, 128.3, 128.8 (2C), 129.8, 130.5, 131.2, 134.0, 136.0, 137.0, 138.1, 139.6, 146.4, 146.5, 151.6, 161.9, 166.8; MS (ESI) *m/z* 382.2 $[M+H]^+$; HRMS: calcd for $C_{21}H_{16}N_7O$ $[M+H]^+$ 382.1416, found 382.1406; HPLC t_R = 5.2 min, 100%.

***2-[3-(1H-Imidazol-4-yl)phenyl]-N-(9H-purin-6-yl)benzamide* (4a):** yield = 2.5%; white powder; ^{1}H NMR (DMSO-d_6): δ = 7.29 (d, 2H, ^{3}J = 9.0 Hz), 7.48-7.56 (m, 3H), 7.61-7.73 (m, 4H), 7.90 (s, 1H), 8.39 (s, 1H), 8.59 (s, 1H), 11.96 (bs, 3H); ^{13}C NMR (DMSO-d_6): δ = 114.6, 115.2, 123.3, 124.4, 126.2, 127.2, 128.2, 128.5, 128.9, 130.0, 130.6, 134.3, 135.2, 136.0, 140.1, 140.2, 144.4, 145.8, 151.1, 161.2, 166.4; MS (ESI) *m/z* 382.1 $[M+H]^+$; HRMS: calcd for $C_{21}H_{16}N_7O$ $[M+H]^+$ 382.1416, found 382.1425; HPLC t_R = 5.0 min, 99.1%.

***2-[4-(1H-Imidazol-4-yl)phenyl]-N-(9H-purin-6-yl)benzamide* (4b):** yield = 5%; white powder; ^{1}H NMR (DMSO-d_6): δ = 7.39-7.71 (m, 10H), 8.42 (s, 1H), 8.60 (s, 1H), 11.52 (bs, 1H), 12.21 ppm (bs, 1H); ^{13}C NMR (DMSO-d_6): δ = 113.4, 115.1, 124.2 (2C), 126.7, 128.7 (4C), 129.9, 130.7, 133.1, 134.8, 136.1, 137.5, 139.9, 144.0, 146.1, 151.2, 162.1, 169.5; MS (ESI) *m/z* 382.2 $[M+H]^+$; HRMS: calcd for $C_{21}H_{16}N_7O$ $[M+H]^+$ 382.1416, found 382.1425; HPLC t_R = 5.0 min, 100%.

***3-[3-(1H-Imidazol-4-yl)phenyl]-N-(9H-purin-6-yl)benzamide* (4c):** yield = 25%; white powder; ^{1}H NMR (DMSO-d_6): δ = 7.50 (t, 1H, ^{3}J = 9.0 Hz), 7.64-7.81 (m, 5H), 8.03 (d, 1H, ^{3}J = 9.0 Hz), 8.11 (d, 1H, ^{3}J = 9.0 Hz), 8.21 (s, 1H), 8.48 (s, 1H), 8.51 (s, 1H), 8.75 (s, 1H), 11.89 (bs, 1H), 12.23 (bs, 1H), 12.66 (bs, 1H); ^{13}C NMR (DMSO-d_6): δ = 113.7, 116.0, 123.2, 124.4, 125.2, 127.3 (2C), 128.1, 129.7 (3C), 131.3, 133.9, 136.5, 140.0, 140.9, 145.6, 146.4, 151.6, 161.7, 167.0; MS (ESI) *m/z*

382.2 $[M+H]^+$; HRMS: calcd for $C_{21}H_{16}N_7O$ $[M+H]^+$ 382.1416, found 382.1411; HPLC t_R = 4.7 min, 98.7%.

***3-[4-(1H-Imidazol-4-yl)phenyl]-N-(9H-purin-6-yl)benzamide* (4d):** yield = 34%; white powder; ^{1}H NMR (DMSO-d_6): δ = 7.67-7.70 (m, 2H), 7.75 (s, 1H), 7.85 (d, 2H, ^3J = 6.0 Hz), 7.91 (d, 2H, ^3J = 6.0 Hz), 8.01 (d, 1H, ^3J = 6.0 Hz), 8.06 (d, 1H, ^3J = 6.0 Hz), 8.49 (s, 1H), 8.52 (s, 1H), 8.76 (s, 1H), 11.77 (bs, 1H), 12.31 (bs, 1H), 12.48 (bs, 1H); ^{13}C NMR (DMSO-d_6): δ = 114.9, 115.8, 125.3(2C), 126.9, 127.5 (2C), 127.9, 129.7, 130.9, 133.9, 134.2, 136.6, 137.2, 138.2, 140.5, 145.0, 146.6, 151.6, 162.6, 167.0; MS (ESI) *m/z* 382.2 $[M+H]^+$; HRMS: calcd for $C_{21}H_{16}N_7O$ $[M+H]^+$ 382.1416, found 382.1427; HPLC t_R = 5.4 min, 100%.

General procedure for the synthesis of compounds 1b-e

To a stirred solution of adenine (3.03 mmol) in pyridine (5 mL) at 100°C was added portionwise, under argon, the corresponding (1,1'-biphenyl)carbonyl chloride **5b-c** or naphtoyl chloride **5d-e** (2.44 mmol). The reaction mixture was stirred at 100°C until TLC revealed that the starting material was consumed. Solvent were removed under reduced pressure and the residue was purified on silica gel column chromatography (CH_2Cl_2/MeOH, 0-10%) to provide compounds **1b-e**.

***3-Phenyl-N-(9H-purin-6-yl)benzamide* (1b):** yield = 78%; white powder; ^{1}H NMR (DMSO-d_6): δ = 7.40-7.45 (m, 1H), 7.50-7.55 (m, 2H), 7.65-7.70 (m, 1H), 7.83-7.85 (d, 2H, ^3J = 6.0 Hz), 7.98 (d, 1H, ^3J = 6.0 Hz), 8.10 (d, 1H, ^3J = 6.0 Hz), 8.45 (s, 1H), 8.51 (s, 1H), 8.75 (s, 1H), 11.70 (bs, 1H), 12.39 (bs, 1H); ^{13}C NMR (DMSO-d_6): δ = 114.4, 126.8, 126.9 (2C), 127.6, 127.9, 129.0 (2C), 129.2,

130.8, 133.4, 139.3, 140.3, 144.6, 146.2, 151.2, 162.1, 166.4; MS (ESI) *m/z* 316.1 $[M+H]^+$; HRMS: calcd for $C_{18}H_{14}N_5O$ $[M+H]^+$ 316.1198, found 382.1195; HPLC t_R = 7.9 min, 100%.

***4-Phenyl-N-(9H-purin-6-yl)benzamide* (1c):** yield = 62%; white powder; ^{1}H NMR (DMSO-d_6): δ = 7.47-7.59 (m, 3H), 7.57 (d, 2H, ^3J = 8.6 Hz), 7.91 (d, 2H, ^3J = 8.6 Hz), 8.25 (d, 2H, ^3J = 8.6 Hz), 8.55 (s, 1H), 8.78 (s, 1H), 12.02 (bs, 2H); ^{13}C NMR (DMSO-d_6): δ = 155.6, 126.7 (2C), 127.00 (2C), 128.4, 129.1 (2C), 129.4 (2C), 131.7, 138.9, 144.1, 145.2, 145.9, 151.2, 161.1, 166.2; MS (ESI) *m/z* 316.1 $[M+H]^+$; HRMS: calcd for $C_{18}H_{14}N_5O$ $[M+H]^+$ 316.1198, found 316.1195; HPLC t_R = 7.7 min, 100%.

***N-(9H-purin-6-yl)-1-naphtamide* (1d):** yield = 61%; white powder; ^{1}H NMR (DMSO-d_6): δ = 7.61-8.40 (m, 7H), 8.54 (s, 1H), 8.72 (s, 1H), 12.1 (bs, 2H); ^{13}C NMR (DMSO-d_6): δ = 168.8, 161.7, 151.6, 146.5, 145.4, 133.7, 132.7, 131.7, 130.3, 128.9, 127.7, 127.6, 126.9, 125.7, 125.4, 116.3; MS (ESI) *m/z* 290.2 $[M+H]^+$; HRMS: calcd for $C_{16}H_{11}N_5O$ $[M+H]^+$ 290.1042, found 290.1044; HPLC t_R = 5.9 min, 100%.

***N-(9H-purin-6-yl)-2-naphtamide* (1e):** yield = 63%; white powder; ^{1}H NMR (DMSO-d_6): ^{1}H NMR (DMSO-d_6): δ = 7.64-7.69 (m, 2H), 8.03-8.16 (m, 4H), 8.54 (s, 1H), 8.77 (s, 1H), 8.82 (s, 1H), 11.5 (bs, 1H), 12.5 (bs, 1H); ^{13}C NMR (DMSO-d_6): δ = 167.1, 161.6, 151.6, 146.3, 145.6, 135.2, 132.4, 130.6, 130.2, 129.7, 128.9, 128.6, 128.2, 127.5, 125.2, 116.0 MS (ESI) *m/z* 290.2 $[M+H]^+$; HRMS: calcd for $C_{16}H_{11}N_5O$ $[M+H]^+$ 290.1042, found 290.1039; HPLC t_R = 6.5 min, 100%.

General procedure for the synthesis of compounds 6a-e

To a stirred solution of compounds **12a-e** (0.96 mmol) in 1,4-dioxane (5 mL) and MeOH (2.4 mL) was added an aqueous solution of NaOH 2M (2.4 mL) and the mixture was stirred at 50°C until

TLC revealed that the starting material was consumed. After cooling, the reaction mixture was acidified until pH 3 with a solution of HCl 1M. Product was extracted with CH_2Cl_2, dried over anhydrous $MgSO_4$ and concentrated *in vacuo* to provide compounds **6a-e**, which were used without further purification.

2-(3-Pyrrol-1-ylphenyl)benzoic acid (**6a**): yield = 93%; orange powder; ^{1}H NMR ($CDCl_3$): δ 6.29 (t, 2H, ^3J = 2.0 Hz), 7.08 (t, 2H, ^3J = 2.0 Hz), 7.10-7.21 (m, 1H), 7.27-7.58 (m, 6H),7.91 (d, 1H, ^3J = 8.0 Hz); MS (ESI) *m/z* 264.1 $[M+H]^+$.

2-(4-Pyrrol-1-ylphenyl)benzoic acid (**6b**): yield = 100%; white powder; ^{1}H NMR (DMSO-d_6): δ 6.34 (t, 2H, ^3J = 2.0 Hz), 7.47-7.58 (m, 3H), 7.64-7.71 (m, 6H), 7.81 (d, 1H, ^3J = 8.0 Hz), 12.91 (bs, 1H); MS (ESI) *m/z* 264.1 $[M+H]^+$.

3-(3-Pyrrol-1-ylphenyl)benzoic acid (**6c**): yield = 99%; light brown powder; ^{1}H NMR (DMSO-d_6): δ 6.34 (t, 2H, ^3J = 2.0 Hz), 7.56-7.67 (m, 6H), 7.91 (s, 1H), 8.00-8.12 (m, 2H), 8.31 (s, 1H); MS (ESI) *m/z* 264.0 $[M+H]^+$.

3-(4-Pyrrol-1-ylphenyl)benzoic acid (**6d**): yield = 100%; white powder; ^{1}H NMR (DMSO-d_6): δ 6.35 (t, 2H, ^3J = 2.0 Hz), 7.49 (t, 2H, ^3J = 2.0 Hz), 7.63-7.87 (m, 5H), 7.89-8.02 (m, 2H), 8.27 (s, 1H), 13.11 (bs, 1H); MS (ESI) *m/z* 264.1 $[M+H]^+$.

4-(3-Pyrrol-1-ylphenyl)benzoic acid (**6e**): yield = 98%; pale yellow powder; ^{1}H NMR (DMSO-d_6): δ 6.34 (t, 2H, ^3J = 2.0 Hz), 7.55-7.66 (m, 5H), 7.94-8.11 (m, 5H), 12.91 (bs, 1H); MS (ESI) *m/z* 264.0 $[M+H]^+$.

4-(4-Pyrrol-1-ylphenyl)benzoic acid (**6f**): In a round bottom flask containing a stirbar and Et_2O (17 mL) was suspended at 0°C potassium *t*-BuOK (8.7 mmol). H_2O was added and the mixture

was stirred for 10 minutes. After addition of compound **12f** the mixture was stirred at room temperature for 3 h. The mixture was cooled with an ice bath and quenched with AcOH. The solution was acidified until pH 3. The organic layer was washed with water, dried over anhydrous $MgSO_4$ and concentrated *in vacuo* to provide compound **6f** in a 78% yield as a white powder; ^{1}H NMR (DMSO-d_6): δ 6.38 (t, 2H, ^3J = 2.0 Hz), 7.58 (t, 2H, ^3J = 2.0 Hz), 7.79 (d, 2H, ^3J = 7.9 Hz), 7.89-7.94 (m, 4H), 8.12 (d, 2H, ^3J = 7.9 Hz), 12.92 (bs, 1H); MS (ESI) *m/z* 264.1 $[M+H]^+$.

General procedure for the synthesis of compounds 7a-d

To a stirred solution of compounds **14a-d** (1.90 mmol) in 1,4 dioxane (8.9 mL) and EtOH (4.3 mL) was added a solution of NaOH 2M (4.75 mL) and the mixture was stirred at 50°C until TLC revealed that the starting material was consumed. After cooling, the reaction mixture was acidified until pH 3 with a solution of HCl 1M and the resulting solution was concentrated *in vacuo*. The residue was purified by silica gel column chromatography (CH_2Cl_2/MeOH, 0-10%) to provide compounds **7a-d**.

***2-(3-Imidazol-1-ylphenyl)benzoic acid* (7a)**: quantitative yield; white powder; ^{1}H NMR (DMSO-d_6): δ 7.45-7.47 (m, 3H), 7.61-7.69 (m, 2H), 7.80-7.90 (m, 4H), 8.36 (s, 1H), 9.73 (s, 1H), 12.94 (bs, 1H); MS (ESI) *m/z* 265.1 $[M+H]^+$.

***2-(4-Imidazol-1-ylphenyl)benzoic acid* (7b)**: quantitative yield; white powder; ^{1}H NMR (DMSO-d_6): δ 7.43 (d, 1H, ^3J = 9.0 Hz), 7.50-7.66 (m, 4H), 7.81-7.92 (m, 4H), 8.34 (s, 1H), 9.74 (s, 1H), 12.90 (bs, 1H); MS (ESI) *m/z* 265.1 $[M+H]^+$.

***3-(3-Imidazol-1-ylphenyl)benzoic acid* (7c)**: quantitative yield; white powder; ^{1}H NMR (DMSO-d_6): δ 7.67 (t, 1H, ^3J = 9.0 Hz), 7.75 (t, 1H, ^3J = 9.0 Hz), 7.85 (d, 1H, ^3J = 9.0 Hz), 7.91 (s, 2H), 8.02

(d, 1H, ^{3}J = 9.0 Hz), 8.08 (d, 1H, ^{3}J = 9.0 Hz), 8.18 (s, 1H), 8.34 (s, 1H), 8.41 (s, 1H), 9.78 (s, 1H), 13.21 (bs, 1H); MS (ESI) *m/z* 265.1 $[M+H]^{+}$.

***3-(4-Imidazol-1-ylphenyl)benzoic acid* (7d)**: quantitative yield; white powder; ^{1}H NMR (DMSO-d_6): δ 7.66 (t, 1H, ^{3}J = 9.0 Hz), 7.90-8.04 (m, 7H), 8.26 (s, 1H,), 8.34 (s, 1H), 9.71 (s, 1H); MS (ESI) *m/z* 265.1 $[M+H]^{+}$.

General procedure for the synthesis of compounds 8a-d

To a stirred solution of compound **18a-d** (1.06 mmol) in 1,4 dioxane (5 mL) and EtOH (2.4 mL) was added a solution of NaOH 2M (2.64 mL) and the mixture was stirred at 50°C until TLC revealed that the starting material was consumed. After cooling, mixture was acidified until pH 3 with a solution of HCl 1M and the resulting solution was concentrated *in vacuo*. The residue was purified by silica gel column chromatography (CH_2Cl_2/MeOH, 0-10%) to provide compounds **8a-d**.

***2-[3-[1-[(4-Methoxyphenyl)(diphenyl)methyl]imidazol-4-yl]phenyl]benzoic acid* (8a)**: yield = 88%; white powder; ^{1}H NMR (DMSO-d_6): δ 3.76 (s, 3H), 6.97 (d, 2H, ^{3}J = 9.0 Hz), 7.08 (d, 2H, ^{3}J = 9.0 Hz), 7.15 (d, 4H, ^{3}J = 9.0 Hz), 7.21-7.31 (m, 3H), 7.36-7.45 (m, 10H), 7.58 (t, 2H, ^{3}J = 9.0 Hz), 7.73 (s, 1H); MS (ESI) *m/z* 265.1, 273.2 $[M+H]^{+}$.

***2-[4-[1-[(4-Methoxyphenyl)(diphenyl)methyl]imidazol-4-yl]phenyl]benzoic acid* (8b)**: yield = 77%; white powder; ^{1}H NMR (DMSO-d_6): δ 3.77 (s, 3H), 6.99 (d, 2H, ^{3}J = 9.0 Hz), 7.09 (d, 2H, ^{3}J = 9.0 Hz), 7.16 (d, 4H, ^{3}J = 9.0 Hz), 7.28 (d, 2H, ^{3}J = 9.0 Hz), 7.37-7.45 (m, 10H), 7.56 (t, 1H, ^{3}J = 9.0 Hz), 7.71 (d, 1H, ^{3}J = 9.0 Hz), 7.77 (d, 2H, ^{3}J = 9.0 Hz), 12.76 (bs, 1H); MS (ESI) *m/z* 265.1, 273.2 $[M+H]^{+}$.

***3-[3-[1-[(4-Methoxyphenyl)(diphenyl)methyl]imidazol-4-yl]phenyl]benzoic acid* (8c)**: yield = 14%; white powder; ^{1}H NMR (DMSO-d_6): δ 3.77 (s, 3H), 6.98 (d, 2H, ^3J = 9.0 Hz), 7.10 (d, 2H, ^3J = 9.0 Hz), 7.17 (d, 4H, ^3J = 9.0 Hz), 7.35-7.46 (m, 8H), 7.50-7.64 (m, 3H), 7.79 (d, 1H, ^3J = 9.0 Hz), 7.94 (d, 2H, ^3J = 9.0 Hz), 8.08 (s, 1H), 8.18 (s, 1H), 12.95 (bs, 1H); MS (ESI) *m/z* 265.2, 273.2 $[M+H]^+$.

***3-[4-[1-[(4-Methoxyphenyl)(diphenyl)methyl]imidazol-4-yl]phenyl]benzoic acid* (8d)**: yield = 96%; white powder; ^{1}H NMR (DMSO-d_6): δ 3.77 (s, 3H), 6.99 (d, 2H, ^3J = 9.0 Hz), 7.09 (d, 2H, ^3J = 9.0 Hz), 7.17 (d, 4H, ^3J = 9.0 Hz), 7.36-7.50 (m, 8H), 7.58 (t, 1H, ^3J = 9.0 Hz), 7.67 (d, 2H, ^3J = 9.0 Hz), 7.86 (d, 2H, ^3J = 9.0 Hz), 7.92 (d, 2H, ^3J = 9.0 Hz), 8.18 (s, 1H), 13.09 (bs, 1H); MS (ESI) *m/z* 265.1, 273.2 $[M+H]^+$.

General procedure for the synthesis of compounds 10a and 10b

In a round bottom flask equipped with a magnetic stirbar and a rubber septum were added copper chloride (0.3 mmol), 3- or 4-bromoiodobenzene **9a** or **9b** (6 mmol), and pyrrole (9 mmol). The flask was purged with argon and 40% aq. nBu$_4$NOH solution (6 mL) was added under argon. The reaction mixture was stirred under argon at 80°C for 36 h. The mixture was cooled to room temperature and partitioned between EtOAc and aq HCl. The organic layer was washed with water, dried over $MgSO_4$, and concentrated *in vacuo*. The residue was purified by silica gel column chromatography (petroleum ether/EtOAc, 0-4%) to provide the desired compounds.

***1-(3-Bromophenyl)-1H-pyrrole* (10a)**: yield = 69%; white powder; ^{1}H NMR ($CDCl_3$): δ 6.30 (s, 2H), 7.00 (s, 2H), 7.12-7.32 (m, 3H), 7.45 (s, 1H); MS (ESI) *m/z* 222.0-224.1 $[M+H]^+$.

***1-(4-Bromophenyl)-1H-pyrrole* (10b)**: yield = 79%; white powder; ^{1}H NMR (DMSO-d_6): δ 6.28 (s, 2H), 7.39 (s, 2H), 7.56 (d, 2H, ^3J = 9.0 Hz), 7.63 (d, 2H, ^3J = 9.0 Hz); MS (ESI) *m/z* 222.0, 224.0 $[M+H]^+$.

General procedure for the synthesis of compounds 11a and 11b

In a round bottom flask equipped with a magnetic stirbar and a rubber septum were added $Pd_2(dba)_3$ (0.016 mmol), compound **10a** or **10b** (1.58 mmol), bis(pinacolato)diboron (1.74 mmol), 2-(dicyclohexylphosphino)-2',4',6'-triisopropylbiphenyl (0.063 mmol) and KOAc (4.74 mmol). The flask was purged with argon and DMF (6 mL) was added under argon. The reaction mixture was stirred under argon at 110°C for 2 h. The mixture was cooled to room temperature, filtered through a pad of celite and the cake was washed with EtOAc. The filtrate was concentrated *in vacuo* and the residue was purified by silica gel column chromatography (petroleum ether/ EtOAc, 0-10%) to provide the desired compounds.

***1-[3-(4,4,5,5-Tetramethyl-1,3,2-dioxaborolan-2-yl)phenyl]-1H-pyrrole* (11a)**: yield = 84%; orange powder; ^{1}H NMR ($CDCl_3$): δ 1.31 (s, 12H), 6.27 (t, 2H, ^3J = 2.0 Hz), 7.06 (t, 2H, ^3J = 2.0 Hz), 7.31-7.45 (m, 2H), 7.61 (m, 1H), 7.76 (d, 1H, ^4J = 2.0 Hz); MS (ESI) *m/z* 270.2 $[M+H]^+$.

***1-[4-(4,4,5,5-Tetramethyl-1,3,2-dioxaborolan-2-yl)phenyl]-1H-pyrrole* (11b)**: yield = 78%; orange powder; ^{1}H NMR ($CDCl_3$): δ 1.28 (s, 12H), 6.28 (t, 2H, ^3J = 2.0 Hz), 7.07 (t, 2H, ^3J = 2.0 Hz), 7.32 (d, 2H, ^3J = 9.0 Hz), 7.78 (d, 2H, ^3J = 9.0 Hz); MS (ESI) *m/z* 270.2 $[M+H]^+$.

General procedure for the synthesis of compounds 12a-f

In a round bottom flask equipped with a magnetic stirbar and a rubber septum were added under argon $Pd_2(dba)_3$ (0.13 mmol), compound **11a** or **11b** (1.55 mmol), the corresponding

methyl-2-bromo, 3-bromo or 4-bromobenzoates (1.29 mmol), K_2CO_3 (3.87 mmol) and DMF (5mL). The reaction mixture was stirred under argon at 100°C for 18 h. The mixture was cooled to room temperature, and diluted with water. The solution was neutralized with HCl 1N and product was extracted with EtOAc. Organic layers were dried over $MgSO_4$, and concentrated *in vacuo*. The residue was purified by silica gel column chromatography (petroleum ether /CH_2Cl_2, 0-80%) to provide compounds **12a-f**.

***Methyl-2-(3-pyrrol-1-ylphenyl)benzoate* (12a)**: yield = 64%; orange oil; ^{1}H NMR ($CDCl_3$): δ 3.62 (s, 3H), 6.30 (t, 2H, ^3J = 2.0 Hz), 7.05-7.18 (m, 3H), 7.28-7.58 (m, 6H), 7.81 (d, 1H, ^3J = 8.0 Hz); MS (ESI) *m/z* 278.1 $[M+H]^+$.

***Methyl-2-(4-pyrrol-1-ylphenyl)benzoate* (12b)**: yield = 41%; white powder; ^{1}H NMR ($CDCl_3$): δ 3.62 (s, 3H), 6.32 (t, 2H, ^3J = 2.0 Hz), 7.11 (t, 2H, ^3J = 2.0 Hz), 7.27-7.57 (m, 7H), 7.80 (d, 1H, ^3J = 7.9 Hz); MS (ESI) *m/z* 278.1 $[M+H]^+$.

***Methyl-3-(3-pyrrol-1-ylphenyl)benzoate* (12c)**: yield = 69%; white powder; ^{1}H NMR ($CDCl_3$): δ 3.90 (s, 3H), 6.35 (t, 2H, ^3J = 2.0 Hz), 7.10 (t, 2H, ^3J = 2.0 Hz), 7.31-7.60 (m, 5H), 7.75 (d, 1H, ^3J = 7.9 Hz), 7.99 (d, 1H, ^3J = 7.9 Hz), 8.23 (s, 1H); MS (ESI) *m/z* 278.1 $[M+H]^+$.

***Methyl-3-(4-pyrrol-1-ylphenyl)benzoate* (12d)**: yield = 66%; pale yellow powder; ^{1}H NMR ($CDCl_3$): δ 3.91 (s, 3H), 6.35 (t, 2H, ^3J = 2.0 Hz), 7.08 (t, 2H, ^3J = 2.0 Hz), 7.41-7.78 (m, 7H), 7.81 (d, 1H, ^3J = 7.9 Hz); MS (ESI) *m/z* 278.1 $[M+H]^+$.

***Methyl-4-(3-pyrrol-1-ylphenyl)benzoate* (12e)**: yield = 71%; white powder; ^{1}H NMR ($CDCl_3$): δ 3.89 (s, 3H), 6.31 (t, 2H, ^3J = 2.0 Hz), 7.08 (t, 2H, ^3J = 2.0 Hz), 7.32-7.46 (m, 3H), 7.54-7.64 (m, 3H), 8.05 (d, 2H, ^3J = 7.9 Hz); MS (ESI) *m/z* 278.1 $[M+H]^+$.

***Methyl-4-(4-pyrrol-1-ylphenyl)benzoate* (12f):** yield = 65%; white powder; ^{1}H NMR ($CDCl_3$): δ 3.89 (s, 3H), 6.32 (t, 2H, ^3J = 2.0 Hz), 7.09 (t, 2H, ^3J = 2.0 Hz), 7.42 (d, 2H, ^3J = 7.9 Hz), 7.57-7.68 (m, 4H), 8.05 (d, 2H, ^3J = 7.9 Hz); MS (ESI) *m/z* 278.0 $[M+H]^+$.

General procedure for the synthesis of compounds 13a and 13b

In a round bottom flask equipped with a magnetic stirbar and a rubber septum were added CuI (0.71 mmol), benzotriazole (1.41 mmol) and DMSO (7 mL). The solution was degassed by argon purging for 30 min and 3- or 4-bromoiodobenzene **9a** or **9b** (7.10 mmol), imidazole (7.10 mmol) and *t*-BuOK were introduced. The reaction mixture was stirred under argon at 100°C for 14 h. The mixture was cooled to room temperature, filtered through a pad of celite and the cake was washed with EtOAc. The filtrate was washed with water, dried over $MgSO_4$, and concentrated *in vacuo*. The residue was purified by silica gel column chromatography (petroleum ether/ EtOAc, 25-100%) to provide the desired compounds.

***1-(3-Bromophenyl)imidazole* (13a)**: yield = 70%; dark red oil; ^{1}H NMR (DMSO-d_6): δ 7.15 (s, 1H), 7.50 (t, 1H, ^3J = 9.0 Hz), 7.55 (dd, 1H, ^3J = 9.0 Hz, ^4J = 3.0 Hz), 7.71 (dd, 1H, ^3J = 9.0 Hz, ^4J = 3.0 Hz), 7.85 (s, 1H), 7.97 (t, 1H, ^4J = 3.0 Hz), 8.39 (s, 1H); MS (ESI) *m/z* 223.0, 225.0 $[M+H]^+$.

***1-(4-Bromophenyl)imidazole* (13b)**: yield = 70%; light brown powder; ^{1}H NMR (DMSO-d_6): δ 7.12 (s, 1H), 7.68 (d, 2H, ^3J = 9.0 Hz), 7.72 (d, 2H, ^3J = 9.0 Hz) 7.77 (s, 1H), 8.29 (s, 1H); MS (ESI) *m/z* 223.0, 225.0 $[M+H]^+$.

General procedure for the synthesis of compounds 14a-d

To a three-neck round-bottom flask under argon atmosphere was added $Pd(PPh_3)_4$ (0.16 mmol), DMF (10.5 mL) and compounds **13a** or **13b** (1.57 mmol). K_2CO_3 (4.71 mmol) and the

corresponding 2-, 3- or 4-ethoxycarbonyl benzeneboronic acids (2.67 mmol) were successively added and the mixture was stirred under argon at 100 °C until TLC revealed that the starting material was consumed. The mixture was cooled to room temperature, diluted with water and product was extracted with EtOAc. Organic layers were dried over $MgSO_4$, concentrated *in vacuo* and the residue was purified by silica gel column chromatography (CH_2Cl_2/MeOH, 0-5%) to provide compounds **14a-d**.

***Ethyl-2-(3-imidazol-1-ylphenyl)benzoate* (14a)**: yield = 76%, light brown oil; ^{1}H NMR ($CDCl_3$): δ 1.06 (t, 3H, ^3J = 6.0 Hz), 4.13 (q, 2H, ^3J = 6.0 Hz), 7.22 (s, 1H), 7.29-7.41 (m, 5H), 7.44-7.60 (m, 4H), 7.91 (d, 1H, ^3J = 9.0 Hz).

***Ethyl-2-(4-imidazol-1-ylphenyl)benzoate* (14b)**: yield = 74%, light brown oil; ^{1}H NMR ($CDCl_3$): δ 1.10 (t, 3H, ^3J = 6.0 Hz), 4.17 (q, 2H, ^3J = 6.0 Hz), 7.23-7.26 (m, 1H), 7.32-7.38 (m, 2H), 7.43-7.70 (m, 7H), 7.91 (d, 1H, ^3J = 9.0 Hz).

***Ethyl-3-(3-imidazol-1-ylphenyl)benzoate* (14c)**: yield = 59%, light brown oil; ^{1}H NMR ($CDCl_3$): δ 1.42 (t, 3H, ^3J = 6.0 Hz), 4.41 (q, 2H, ^3J = 6.0 Hz), 7.35-7.36 (m, 2H), 7.40-7.70 (m, 5H), 7.78 (d, 1H, ^3J = 9.0 Hz), 8.06-8.10 (m, 2H), 8.29 (s, 1H).

***Ethyl-3-(4-imidazol-1-ylphenyl)benzoate* (14d)**: yield = 51%, light brown oil; ^{1}H NMR ($CDCl_3$): δ 1.40 (t, 3H, ^3J = 6.0 Hz), 4.41 (q, 2H, ^3J = 6.0 Hz), 7.46-7.80 (m, 8H), 7.96 (s, 1H), 8.07 (d, 1H, ^3J = 6.0 Hz), 8.29 (s, 1H).

***4-(3-Bromophenyl)-1H-imidazole 16a*:**

In a round bottom flask equipped with a magnetic stirbar were added 2,3'-dibromoacetophenone **15** (10.79 mmol) and formamide (2.02 mol). The reaction mixture was

stirred at 170°C for 14 h. The mixture was cooled to room temperature and diluted with a saturated solution of $NaHCO_3$. Product was extracted with EtOAc, organic layers were dried over $MgSO_4$ and concentrated *in vacuo*. The residue was purified by silica gel column chromatography (petroleum ether/ EtOAc, 12-100%) to provide compounds **16a** in a 54% yield as a light brown powder; ^{1}H NMR (DMSO-d_6): δ 7.28-7.38 (m, 2H), 7.71-7.78 (m, 3H), 7.96 (s, 1H), 12.29 (bs, 1H); MS (ESI) *m/z* 223.0, 225.0 $[M+H]^+$.

General procedure for the synthesis of compounds 17a and 17b

To a stirred solution of compound **16a** or **16b** (4.48 mmol) in DMF (30 mL) were added under argon triethylamine (6.72 mmol) and 4-monomethoxytrityl chloride (5.38 mmol). The solution was stirred under argon for 2h, then diluted with water and product was extracted with EtOAc. Organic layers were dried over $MgSO_4$, concentrated *in vacuo* and the residue was purified by silica gel column chromatography (petroleum ether/ EtOAc, 5-40%) to provide compounds **17a-b**.

4-(3-Bromophenyl)-1-[(4-methoxyphenyl)(diphenyl)methyl]imidazole **(17a)**: yield = 96%; white powder; ^{1}H NMR (DMSO-d_6): δ 3.77 (s, 3H), 6.97 (d, 2H, ^3J = 9.0 Hz), 7.07 (d, 2H, ^3J = 9.0 Hz), 7.15 (d, 4H, ^3J = 9.0 Hz), 7.26 (t, 1H, ^3J = 9.0 Hz), 7.35-7.45 (m, 8H), 7.61 (s, 1H), 7.76 (d, 1H, ^3J = 9.0 Hz), 7.97 (s, 1H); MS (ESI) *m/z* 223.1, 225.1, 273.2 $[M+H]^+$.

4-(4-Bromophenyl)-1-[(4-methoxyphenyl)(diphenyl)methyl]imidazole **(17b)**: yield = 98%; white powder; ^{1}H NMR (DMSO-d_6): δ 3.77 (s, 3H), 6.97 (d, 2H, ^3J = 9.0 Hz), 7.07 (d, 2H, ^3J = 9.0 Hz), 7.15 (d, 4H, ^3J = 9.0 Hz), 7.35-7.50 (m, 10H), 7.71 (d, 2H, ^3J = 9.0 Hz); MS (ESI) *m/z* 223.1, 225.1, 273.2 $[M+H]^+$.

General procedure for the synthesis of compounds 18a-d

To a three-neck round-bottom flask under argon atmosphere was added $Pd(PPh_3)_4$ (0.14 mmol), DMF (9.5 mL) and compounds **17a-b** (1.41 mmol). K_2CO_3 (4.24 mmol) and the corresponding 2-, or 3-, or 4-ethoxycarbonylbenzeneboronic acid (2.40 mmol) were successively added and the reaction mixture was stirred under argon at 100 °C until TLC revealed that the starting material was consumed. The mixture was cooled to room temperature, diluted with water and product was extracted with EtOAc. Organic layers were dried over $MgSO_4$, concentrated *in vacuo* and the residue was purified by silica gel column chromatography (petroleum ether/ EtOAc, 0-60%) to provide the desired compounds.

Ethyl-2-[3-[1-[(4-methoxyphenyl)(diphenyl)methyl]imidazol-4-yl]phenyl]benzoate **(18a)**: yield = 62%; white powder; ^{1}H NMR (DMSO-d_6): δ 0.92 (t, 3H, ^3J = 6.0 Hz), 3.77 (s, 3H), 4.00 (q, 2H, ^3J = 6.0 Hz), 6.97 (d, 2H, ^3J = 9.0 Hz), 7.08 (d, 2H, ^3J = 9.0 Hz), 7.15 (d, 4H, ^3J = 9.0 Hz), 7.23 (d, 2H, ^3J = 9.0 Hz), 7.36-7.50 (m, 10H), 7.58 (d, 1H, ^3J = 9.0 Hz), 7.68-7.78 (m, 3H); MS (ESI) *m/z* 273.2, 293.2 $[M+H]^+$.

Ethyl-2-[4-[1-[(4-methoxyphenyl)(diphenyl)methyl]imidazol-4-yl]phenyl]benzoate **(18b)**: yield = 66%; pale yellow powder; ^{1}H NMR (DMSO-d_6): δ 1.02 (t, 3H, ^3J = 6.0 Hz), 3.77 (s, 3H), 4.06 (q, 2H, ^3J = 6.0 Hz), 6.99 (d, 2H, ^3J = 9.0 Hz), 7.09 (d, 2H, ^3J = 9.0 Hz), 7.16 (d, 4H, ^3J = 9.0 Hz), 7.24 (d, 2H, ^3J = 9.0 Hz), 7.38-7.50 (m, 10H), 7.61 (t, 1H, ^3J = 9.0 Hz), 7.70 (d, 1H, ^3J = 9.0 Hz), 7.79 (d, 2H, ^3J = 9.0 Hz); MS (ESI) *m/z* 273.2, 293.2 $[M+H]^+$.

Ethyl-3-[3-[1-[(4-methoxyphenyl)(diphenyl)methyl]imidazol-4-yl]phenyl]benzoate **(18c)**: yield = 51%; white powder; ^{1}H NMR (DMSO-d_6): δ 1.34 (t, 3H, ^3J = 6.0 Hz), 3.77 (s, 3H), 4.35 (q, 2H, ^3J =

6.0 Hz), 6.98 (d, 2H, ^3J = 9.0 Hz), 7.10 (d, 2H, ^3J = 9.0 Hz), 7.17 (d, 4H, ^3J = 9.0 Hz), 7.35-7.53 (m, 9H), 7.58-7.64 (m, 2H), 7.80 (d, 1H, ^3J = 9.0 Hz), 7.96 (t, 2H, ^3J = 9.0 Hz), 8.08 (s, 1H), 8.18 (s, 1H); MS (ESI) *m/z* 273.2, 293.2 $[M+H]^+$.

Ethyl-3-[4-[1-[(4-methoxyphenyl)(diphenyl)methyl]imidazol-4-yl]phenyl]benzoate **(18d)**: yield = 43%; white powder; ^{1}H NMR (DMSO-d_6): δ 1.34 (t, 3H, ^3J = 6.0 Hz), 3.77 (s, 3H), 4.35 (q, 2H, ^3J = 6.0 Hz), 6.99 (d, 2H, ^3J = 9.0 Hz), 7.09 (d, 2H, ^3J = 9.0 Hz), 7.17 (d, 4H, ^3J = 9.0 Hz), 7.38-7.50 (m, 8H), 7.61 (t, 1H, ^3J = 9.0 Hz), 7.67 (d, 2H, ^3J = 9.0 Hz), 7.87 (d, 2H, ^3J = 9.0 Hz), 7.95 (t, 2H, ^3J = 9.0 Hz), 8.18 (s, 1H); MS (ESI) *m/z* 273.2, 293.2 $[M+H]^+$.

ASSOCIATED CONTENT

Supporting Information

Details of experimental procedures for *in vitro* and biological assays, additional figures illustrating NMR screening, synthesis pathways, X-ray data collection and copies of ^{1}H NMR, ^{13}C NMR and ESI-MS Spectra of final compounds. This material is available free of charge via the Internet at http://pubs.acs.org.

Accession Codes

5CR7 (cN-II-**2c**), 5CQZ (cN-II-**3c**).

AUTHOR INFORMATION

Corresponding Author

*Phone: (+33)-4-3435-9465. Fax: (+33)-4-3435-9465. Email: laurent.chaloin@cpbs.cnrs.fr

Author Contributions

¶ Z.M. and R.G. contributed equally to this work.

Notes

The authors declare no competing financial interest.

ACKNOWLEDGMENTS

This work was supported by Institutional funds from the Région Languedoc-Roussillon (Program Chercheurs d'Avenir), the Institut National du Cancer (INCa, project n°2010-200 "Nucleotarg") and the Agence Nationale de la Recherche (ANR Programme Blanc 2011-SIMI7, "cN-II Focus"). We thank J. Viguier and L. Carrique for their contribution in the project, E. Cros-Perrial, F. Galisson and J. Gobbi for excellent technical assistance.

ABBREVIATIONS USED

ALL, Acute lymphoblastic leukemia; AML, Acute myeloid leukemia; Ap_4A, Diadenosine tetraphosphate; ATP, Adenosine 5'-triphosphate; BPG, 2,3-Bisphosphoglycerate; cN-II, Cytosolic 5'-nucleotidase II; FBDD, Fragment-based drug design; INPHARMA, Interligand NOEs for pharmacophore mapping; IMP, Inosine 5'-monophosphate; NMR, Nuclear magnetic resonance;

STD, Saturation transfer difference; Waterlogsy, Water-ligand observed *via* gradient spectroscopy.

REFERENCES

(1) Chen, Y.; Shoichet, B. K. Molecular docking and ligand specificity in fragment-based inhibitor discovery. *Nat. Chem. Biol.* **2009**, *5*, 358-364.

(2) Hajduk, P. J.; Greer, J. A decade of fragment-based drug design: strategic advances and lessons learned. *Nat. Rev. Drug. Discov.* **2007**, *6*, 211-219.

(3) Kumar, A.; Voet, A.; Zhang, K. Y. Fragment based drug design: from experimental to computational approaches. *Curr. Med. Chem.* **2012**, *19*, 5128-5147.

(4) Murray, C. W.; Rees, D. C. The rise of fragment-based drug discovery. *Nat. Chem.* **2009**, *1*, 187-192.

(5) Erlanson, D. A. Introduction to fragment-based drug discovery. *Top. Curr. Chem.* **2012**, *317*, 1-32.

(6) Chen, H.; Zhou, X.; Wang, A.; Zheng, Y.; Gao, Y.; Zhou, J. Evolutions in fragment-based drug design: the deconstruction-reconstruction approach. *Drug Discov. Today* **2015**, *20*, 105-113.

(7) Kim, H. Y.; Wyss, D. F. NMR screening in fragment-based drug design: a practical guide. *Methods Mol. Biol.* **2015**, *1263*, 197-208.

(8) Hennig, M.; Ruf, A.; Huber, W. Combining biophysical screening and X-ray crystallography for fragment-based drug discovery. *Top. Curr. Chem.* **2012**, *317*, 115-143.

(9) Congreve, M.; Langmead, C.; Marshall, F. H. The use of GPCR structures in drug design. *Adv. Pharmacol.* **2011**, *62*, 1-36.

(10) Congreve, M.; Rich, R. L.; Myszka, D. G.; Figaroa, F.; Siegal, G.; Marshall, F. H. Fragment screening of stabilized G-protein-coupled receptors using biophysical methods. *Methods Enzymol.* **2011**, *493*, 115-136.

(11) Chen, L.; Cressina, E.; Leeper, F. J.; Smith, A. G.; Abell, C. A fragment-based approach to identifying ligands for riboswitches. *ACS Chem. Biol.* **2010**, *5*, 355-358.

(12) Feder, D.; Hussein, W. M.; Clayton, D. J.; Kan, M. W.; Schenk, G.; McGeary, R. P.; Guddat, L. W. Identification of purple acid phosphatase inhibitors by fragment-based screening: promising new leads for osteoporosis therapeutics. *Chem. Biol. Drug Des.* **2012**, *80*, 665-674.

(13) Mohd-Pahmi, S. H.; Hussein, W. M.; Schenk, G.; McGeary, R. P. Synthesis, modelling and kinetic assays of potent inhibitors of purple acid phosphatase. *Bioorg. Med. Chem. Lett.* **2011**, *21*, 3092-3094.

(14) Jordheim, L. P.; Chaloin, L. Therapeutic perspectives for cN-II in cancer. *Curr. Med. Chem.* **2013**, *20*, 4292-4303.

(15) Galmarini, C. M.; Graham, K.; Thomas, X.; Calvo, F.; Rousselot, P.; El Jafaari, A.; Cros, E.; Mackey, J. R.; Dumontet, C. Expression of high Km 5'-nucleotidase in leukemic blasts is an independent prognostic factor in adults with acute myeloid leukemia. *Blood* **2001**, *98*, 1922-1926.

(16) Cros, E.; Jordheim, L.; Dumontet, C.; Galmarini, C. M. Problems related to resistance to cytarabine in acute myeloid leukemia. *Leuk. Lymphoma* **2004**, *45*, 1123-1132.

(17) Tzoneva, G.; Perez-Garcia, A.; Carpenter, Z.; Khiabanian, H.; Tosello, V.; Allegretta, M.; Paietta, E.; Racevskis, J.; Rowe, J. M.; Tallman, M. S.; Paganin, M.; Basso, G.; Hof, J.; Kirschner-Schwabe, R.; Palomero, T.; Rabadan, R.; Ferrando, A. Activating mutations in the NT5C2 nucleotidase gene drive chemotherapy resistance in relapsed ALL. *Nat. Med.* **2013**, *19*, 368-371.

(18) Meyer, J. A.; Wang, J.; Hogan, L. E.; Yang, J. J.; Dandekar, S.; Patel, J. P.; Tang, Z.; Zumbo, P.; Li, S.; Zavadil, J.; Levine, R. L.; Cardozo, T.; Hunger, S. P.; Raetz, E. A.; Evans, W. E.; Morrison, D. J.; Mason, C. E.; Carroll, W. L. Relapse-specific mutations in NT5C2 in childhood acute lymphoblastic leukemia. *Nat. Genet.* **2013**, *45*, 290-294.

(19) Gallier, F.; Lallemand, P.; Meurillon, M.; Jordheim, L. P.; Dumontet, C.; Perigaud, C.; Lionne, C.; Peyrottes, S.; Chaloin, L. Structural insights into the inhibition of cytosolic 5'-nucleotidase II (cN-II) by ribonucleoside 5'-monophosphate analogues. *PLoS Comp. Biol.* **2011**, *7*, e1002295.

(20) Meurillon, M.; Marton, Z.; Hospital, A.; Jordheim, L. P.; Bejaud, J.; Lionne, C.; Dumontet, C.; Perigaud, C.; Chaloin, L.; Peyrottes, S. Structure-activity relationships of beta-hydroxyphosphonate nucleoside analogues as cytosolic 5'-nucleotidase II potential inhibitors: synthesis, in vitro evaluation and molecular modeling studies. *Eur. J. Med. Chem.* **2014**, *77*, 18-37.

(21) Cividini, F.; Pesi, R.; Chaloin, L.; Allegrini, S.; Camici, M.; Cros-Perrial, E.; Dumontet, C.; Jordheim, L. P.; Tozzi, M. G. The purine analog fludarabine acts as a cytosolic 5'-nucleotidase II inhibitor. *Biochem. Pharmacol.* **2015**, *94*, 63-68.

(22) Pesi, R.; Allegrini, S.; Careddu, M. G.; Filoni, D. N.; Camici, M.; Tozzi, M. G. Active and regulatory sites of cytosolic 5'-nucleotidase. *FEBS J.* **2010**, *277*, 4863-4872.

(23) Wallden, K.; Rinaldo-Matthis, A.; Ruzzenente, B.; Rampazzo, C.; Bianchi, V.; Nordlund, P. Crystal structures of human and murine deoxyribonucleotidases: insights into recognition of substrates and nucleotide analogues. *Biochemistry* **2007**, *46*, 13809-13818.

(24) Jordheim, L. P.; Marton, Z.; Rhimi, M.; Cros-Perrial, E.; Lionne, C.; Peyrottes, S.; Dumontet, C.; Aghajari, N.; Chaloin, L. Identification and characterization of inhibitors of cytoplasmic 5'-nucleotidase cN-II issued from virtual screening. *Biochem. Pharmacol.* **2013**, *85*, 497-506.

(25) Bhardwaj, V.; Gumber, D.; Abbot, V.; Dhiman, S.; Sharma, P. Pyrrole: a resourceful small molecule in key medicinal hetero-aromatics. *RSC Adv.* **2015**, *5*, 15233-15266.

(26) Verma, A. K.; Singh, J.; Sankar, V. K.; Chaudhary, R.; Chandra, R. Benzotriazole: an excellent ligand for Cu-catalyzed N-arylation of imidazoles with aryl and heteroaryl halides. *Tetrahedron Lett.* **2007**, *48*, 4207-4210.

(27) Xu, H. J.; Zheng, F. Y.; Liang, Y. F.; Cai, Z. Y.; Feng, Y. S.; Che, D. Q. Ligand-free CuCl-catalyzed C-N bond formation in aqueous media. *Tetrahedron Lett.* **2010**, *51*, 669-671.

(28) Heiskanen, J. P.; Hormi, O. E. O. 4-Aryl-8-hydroxyquinolines from 4-chloro-8-tosyloxyquinoline using a Suzuki-Miyaura cross-coupling approach. *Tetrahedron* **2009**, *65*, 518-524.

(29) Billingsley, K. L.; Barder, T. E.; Buchwald, S. L. Palladium-catalyzed borylation of aryl chlorides: Scope, applications, and computational studies. *Angew. Chem. Int. Ed.* **2007**, *46*, 5359-5363.

(30) Young, M. B.; Barrow, J. C.; Glass, K. L.; Lundell, G. F.; Newton, C. L.; Pellicore, J. M.; Rittle, K. E.; Selnick, H. G.; Stauffer, K. J.; Vacca, J. P.; Williams, P. D.; Bohn, D.; Clayton, F. C.;

Cook, J. J.; Krueger, J. A.; Kuo, L. C.; Lewis, S. D.; Lucas, B. J.; McMasters, D. R.; Miller-Stein, C.; Pietrak, B. L.; Wallace, A. A.; White, R. B.; Wong, B.; Yan, Y.; Nantermet, P. G. Discovery and evaluation of potent P1 aryl heterocycle-based thrombin inhibitors. *J. Med. Chem.* **2004**, *47*, 2995-3008.

(31) Weitman, M.; Lerman, L.; Cohen, S.; Nudelman, A.; Major, D. T.; Gottlieb, H. E. Facile structural elucidation of imidazoles and oxazoles based on NMR spectroscopy and quantum mechanical calculations. *Tetrahedron* **2010**, *66*, 1465-1471.

(32) Cividini, F.; Cros-Perrial, E.; Pesi, R.; Machon, C.; Allegrini, S.; Camici, M.; Dumontet, C.; Jordheim, L. P.; Tozzi, M. G. Cell proliferation and drug sensitivity of human glioblastoma cells are altered by the stable modulation of cytosolic 5'-nucleotidase II. *Int. J. Biochem. Cell Biol.* **2015**, *65*, 222-229.

(33) Jordheim, L. P.; Puy, J. Y.; Cros-Perrial, E.; Peyrottes, S.; Lefebvre, I.; Perigaud, C.; Dumontet, C. Determination of the enzymatic activity of cytosolic 5'-nucleotidase cN-II in cancer cells: development of a simple analytical method and related cell line models. *Anal. Bioanal. Chem.* **2015**, *407*, 5747-5758.

(34) Wallden, K.; Stenmark, P.; Nyman, T.; Flodin, S.; Graslund, S.; Loppnau, P.; Bianchi, V.; Nordlund, P. Crystal structure of human cytosolic 5'-nucleotidase II: insights into allosteric regulation and substrate recognition. *J. Biol. Chem.* **2007**, *282*, 17828-17836.

(35) Krissinel, E.; Henrick, K. Inference of macromolecular assemblies from crystalline state. *J. Mol. Biol.* **2007**, *372*, 774-797.

(36) Wallden, K.; Nordlund, P. Structural basis for the allosteric regulation and substrate recognition of human cytosolic 5'-nucleotidase II. *J. Mol. Biol.* **2011**, *408*, 684-696.

(37) Jordheim, L. P.; Cros, E.; Galmarini, C. M.; Dumontet, C.; Bretonnet, A. S.; Krimm, I.; Lancelin, J. M.; Gagnieu, M. C. F-ara-AMP is a substrate of cytoplasmic 5'-nucleotidase II (cN-II): HPLC and NMR studies of enzymatic dephosphorylation. *Nucleosides Nucleotides Nucleic Acids* **2006**, *25*, 289-297.

(38) Bennett, M. J.; Schlunegger, M. P.; Eisenberg, D. 3D domain swapping: a mechanism for oligomer assembly. *Protein Sci.* **1995**, *4*, 2455-2468.

(39) Liu, Y.; Eisenberg, D. 3D domain swapping: as domains continue to swap. *Protein Sci.* **2002**, *11*, 1285-1299.

(40) McGeary, R. P.; Schenk, G.; Guddat, L. W. The applications of binuclear metallohydrolases in medicine: recent advances in the design and development of novel drug leads for purple acid phosphatases, metallo-beta-lactamases and arginases. *Eur. J. Med. Chem.* **2014**, *76*, 132-144.

(41) Barelier, S.; Linard, D.; Pons, J.; Clippe, A.; Knoops, B.; Lancelin, J. M.; Krimm, I. Discovery of fragment molecules that bind the human peroxiredoxin 5 active site. *PLoS One* **2010**, *5*, e9744.

(42) Spychala, J.; Chen, V.; Oka, J.; Mitchell, B. S. ATP and phosphate reciprocally affect subunit association of human recombinant High Km 5'-nucleotidase. Role for the C-terminal polyglutamic acid tract in subunit association and catalytic activity. *Eur. J. Biochem.* **1999**, *259*, 851-858.

(43) Chou, T. C.; Talalay, P. Quantitative analysis of dose-effect relationships: the combined effects of multiple drugs or enzyme inhibitors. *Adv. Enzyme Regul.* **1984**, *22*, 27-55.

Table of Contents Graphic